5

Non-Hertzian normal contact of elastic bodies

The assumptions and restrictions made in the Hertz theory of elastic contact were outlined in the previous chapter: parabolic profiles, frictionless surfaces, elastic half-space theory. In this chapter some problems of normal elastic contact are considered in which we relax one or more of these restrictions. Before looking at particular situations, however, it is instructive to examine the stress conditions which may arise close to the edge of contact.

5.1 Stress conditions at the edge of contact

We have seen in Chapter 4 that, when two non-conforming elastic bodies having continuous profiles are pressed into contact, the pressure distribution between them is not determined uniquely by the profiles of the bodies *within* the contact area. Two further conditions have to be satisfied: (i) that the interface should not carry any tension and (ii) that the surfaces should not interfere *outside* the contact area. These conditions eliminate terms in the pressure distribution of the form $C(1-x^2/a^2)^{-1/2}$ which give rise to an infinite tension or compression at the edge of the contact area ($x = \pm a$) (see equation (4.41)). The resulting pressure distribution was found to be semi-ellipsoidal, i.e. of the form $p_0(1-x^2/a^2)^{1/2}$, which falls to zero at $x = \pm a$.

If we now recall the stresses produced in line loading by a *uniform* distribution of pressure (§2.5), they are everywhere finite, but the gradient of the surface is infinite at the edge of the contact (eq. (2.30*b*) and Fig. 2.8). This infinite gradient of the surface is associated with the jump in pressure from zero outside to p inside the contact. It is clear that two surfaces, initially smooth and continuous, could not deform in this way without interference outside the loaded area. These observations lead to an important principle: *the pressure distribution between two elastic bodies, whose profiles are continuous through*

https://doi.org/10.1017/CBO9781139171731.006 Published online by Cambridge University Press

the boundary of the contact area, falls continuously to zero at the boundary.†

The examples cited in support of this statement were for frictionless surfaces, but it may be shown that the principle is still true if there is slipping friction at the edge of the contact such that $q = \mu p$ and also if friction is sufficient to prevent slip entirely.

If one or both of the bodies has a discontinuous profile at the edge of the contact the situation is quite different and, in general, a high stress concentration would be expected at the edge. The case of a rigid flat punch with square corners was examined in §2.8. For a frictionless punch the pressure distribution was of the form $p_0(1 - x^2/a^2)^{-1/2}$ which, at a small distance ρ from one of the corners, may be written $p_0(2\rho/a)^{-1/2}$. It is recognised, of course, that this infinite stress cannot exist in reality. Firstly, the linear theory of elasticity which gave rise to that result is only valid for small strains and, secondly, real materials will yield plastically at a finite stress. Nevertheless, as developments in linear elastic fracture mechanics have shown, the strength of stress singularities calculated by linear elastic theory is capable of providing useful information about the intensity of stress concentrations and the probable extent of plastic flow.

The conditions at the edge of the contact of a rigid punch with an elastic half-space are influenced by friction on the face of the punch and also by the value of Poisson's ratio for the half-space. If friction prevents slip entirely the pressure and traction on the face of the punch are given by equation (2.69). Close to a corner ($\rho = a - x \ll a$) the pressure distribution may be written

$$p(\rho) = \frac{2(1-\nu)}{\pi(3-4\nu)} (2a\rho)^{-1/2} \cos\{\eta \ln (2a/\rho)\} \tag{5.1}$$

where $\eta = (1/2\pi) \ln (3 - 4\nu)$. This remarkable singularity exhibits an oscillation in pressure at the corner of the punch ($\rho \to 0$).

For an incompressible half-space, however, $\nu = 0.5, \eta = 0$ and the pressure distribution reverts to that without friction. It was shown in §2.8 that, in the absence of an adhesive, the surfaces must slip. The form of the pressure distribution close to the edge of the punch may then be obtained from equation (2.75) to give

$$p(\rho) = \frac{P \cos(\pi\gamma)}{\pi} (2a\rho)^{-1/2} (2a/\rho)^{\pm\gamma} \tag{5.2}$$

where $\tan(\pi\gamma) = -\mu(1 - 2\nu)/2(1 - \nu)$. When either the coefficient of friction is zero or Poisson's ratio is 0.5, $\gamma = 0$ and the pressure distribution reverts to the frictionless form.

† This principle was appreciated by Boussinesq (1885).

https://doi.org/10.1017/CBO9781139171731.006 Published online by Cambridge University Press

In the above discussion we have examined the stress concentration produced by a rigid punch with a square corner. The question now arises: how would that stress concentration be influenced if the punch were also elastic and the angle at the corner were other than 90°? This question has been investigated by Dundurs & Lee (1972) for frictionless contact, by Gdoutos & Theocaris (1975) and Comninou (1976) for frictional contacts, and by Bogy (1971) for no slip. They analyse the state of stress in a two-dimensional elastic wedge of angle ϕ, which has one face pressed into contact with an elastic half-space as shown in Fig. 5.1. The half-space itself may be thought of as a second wedge of angle π. The variation of the stress components with ρ close to the apex of the wedge may take one of the following forms:

(*a*) ρ^{s-1}, if s is real and $0 < s < 1$;
(*b*) $\rho^{\xi-1} \cos(\eta \ln \rho)$ or $\rho^{\xi-1} \sin(\eta \ln \rho)$, if $s = \xi + i\eta$ is complex and $0 < \xi < 1$;
(*c*) $\ln \rho$;
(*d*) constant (including zero);

depending upon the elastic constants of the wedge and half-space, the angle of the wedge ϕ and the frictional conditions at the interface. Dundurs shows that the influence of the elastic constants is governed by only two independent variables:

$$\alpha \equiv \frac{\{(1-\nu_1)/G_1\} - \{(1-\nu_2)/G_2\}}{\{(1-\nu_1)/G_1\} + \{(1-\nu_2)/G_2\}} \tag{5.3a}$$

Fig. 5.1

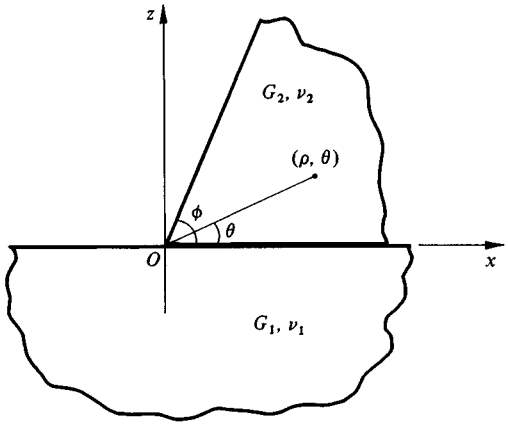

https://doi.org/10.1017/CBO9781139171731.006 Published online by Cambridge University Press

and

$$\beta \equiv \tfrac{1}{2}\left[\frac{\{(1-2\nu_1)/G_1\}-\{(1-2\nu_2)/G_2\}}{\{(1-\nu_1)/G_1\}+\{(1-\nu_2)/G_2\}}\right] \tag{5.3b}$$

α is a measure of the difference in 'plane strain modulus' $\{(1-\nu^2)/E\}$; it varies from -1.0 when the half-space is rigid to $+1.0$ when the wedge is rigid. β has extreme values $\pm\frac{1}{2}$ when one body is rigid and the other has zero Poisson's ratio. If both bodies are incompressible $\beta = 0$. Some typical values of α and β are given in Table 5.1 from which it may be seen that $|\beta|$ seldom exceeds 0.25.

When there is slip between the wedge and the half-space the stresses at the apex may be of the form (*a*), (*c*) or (*d*) as defined above, but complex values of s which lead to oscillating stresses do not arise. For the pressure to be finite at O (case (*d*)) it is found that

$$\alpha \leqslant \frac{(\pi+\phi)\cos\phi+(\mu\pi-1)\sin\phi}{(\pi-\phi)\cos\phi+(\mu\pi+1)\sin\phi} \tag{5.4}$$

Unless the pressure actually falls to zero at O, however, the tangential stress σ in the half-space has a logarithmic singularity at O (case (*c*)). This was found to be the case with a uniform pressure as shown in equation (2.31*a*) and Fig. 2.9. If α exceeds the right-hand side of equation (5.4) there is a power law singularity in pressure at O with the value of s depending upon the values of α, β, ϕ and μ. In this expression the wedge is taken to be slipping relative to the half-space in the positive direction of x, i.e. from left to right in Fig. 5.1. For slip in the opposite direction *negative* values of μ should be used in equation (5.4). The stress concentration at O is reduced by positive sliding and increased by negative sliding. As might be expected, the stress concentration increases with increasing wedge angle ϕ. When the wedge is effectively bonded to the half-space then the stress is always infinite at O. For larger values of $|\alpha|$ and $|\beta|$, s may be complex (case (*b*)) and the pressure and shear traction both

Table 5.1

Body 1	Body 2	G_1 (GPa)	ν_1	G_2 (GPa)	ν_2	α	β
Rubber	metal	$\ll G_2$	0.50	$\gg G_1$	–	1.00	0
Perspex	steel	0.97	0.38	80	0.30	0.97	0.19
Glass	steel	22	0.25	80	0.30	0.57	0.21
Duralumin	steel	28	0.32	80	0.30	0.61	0.12
Cast iron	steel	45	0.25	80	0.30	0.31	0.12
Tungsten carbide	steel	300	0.22	80	0.30	−0.54	−0.24

https://doi.org/10.1017/CBO9781139171731.006 Published online by Cambridge University Press

oscillate close to O. For smaller values of $|\alpha|$ and $|\beta|$, s is real and a power singularity arises (case (a)). To find the value of s in any particular case the reader is referred to the papers cited.

By way of example we shall consider a rectangular elastic block, or an elastic cylinder with flat ends, compressed between two half-spaces. The distributions of pressure and frictional traction on the faces of the block or cylinder have been found by Khadem & O'Connor (1969*a*, *b*) for (*a*) no slip (bonded) and (*b*) no friction at the interface. Close to the edges of contact the stress conditions for both the rectangular block and the cylinder can be determined by reference to the two-dimensional wedge discussed above, with a wedge angle $\phi = 90°$. If the block is rigid and the half-spaces are elastic with $\nu = 0.3$ ($\alpha = 1.0; \beta = 0.286$) the situation is that of a rigid punch discussed in §2.8. In the absence of friction the pressure near the corner varies as $\rho^{-0.5}$ as given by equation (2.64). Points on the interface move tangentially inwards towards the centre of the punch, corresponding to *negative* slip as defined above so that, if the motion is resisted by finite friction ($\mu = -0.5$ say), the stress near the corner varies as $\rho^{-0.45}$, given by equation (5.2). With an infinite friction coefficient, so that all slip is prevented, s is complex and the pressure oscillates as given by equations (2.69) and (5.1).

If now we consider the reverse situation, in which the block is elastic ($\nu = 0.3$) and the half-spaces are rigid ($\alpha = -1, \beta = -0.286$), in the absence of friction the pressure on a face of the block will be uniform. Through Poisson's ratio it will expand laterally so that the slip at a corner is again negative. When this slip is resisted by friction ($\mu = -0.5$) the stress at a corner varies as $\rho^{-0.43}$; if slip is completely prevented it varies as $\rho^{-0.29}$.

Finally we consider block and half-spaces of identical materials so that $\alpha = \beta = 0$. For all frictional conditions the pressure is infinite at the edges: without friction it varies as $\rho^{-0.23}$; with slipping friction, taking $\mu = -0.5$, it varies as $\rho^{-0.44}$. With no slip s is again real and the pressure varies as $\rho^{-0.45}$.

5.2 Blunt wedges and cones

The Hertz theory of contact is restricted to surfaces whose profiles are smooth and continuous; in consequence the stresses are finite everywhere. A rigid punch having sharp square corners, on the other hand, was shown in §2.8 to introduce an infinite pressure at the edges of the contact. In this section we examine the influence of a sharp discontinuity in the *slope* of the profile within the contact area by reference to the contact of a wedge or cone with plane surface. In order for the deformations to be sufficiently small to lie within the scope of the linear theory of elasticity, the semi-angle α of the wedge or cone must be close to 90°.

If we take a two-dimensional wedge indenting a flat surface such that the width of the contact strip is small compared with the size of the two solids then we can use the elastic solutions for a half-space for both wedge and plane surface. The deformation is shown in Fig. 5.2(*a*). The normal displacements are related to the wedge profile by

$$\bar{u}_{z1} + \bar{u}_{z2} = \delta - \cot \alpha \, |x|, \quad -a < x < a \tag{5.5}$$

Fig. 5.2. Indentation by a blunt wedge: (*a*) pressure distribution; (*b*) photo-elastic fringes.

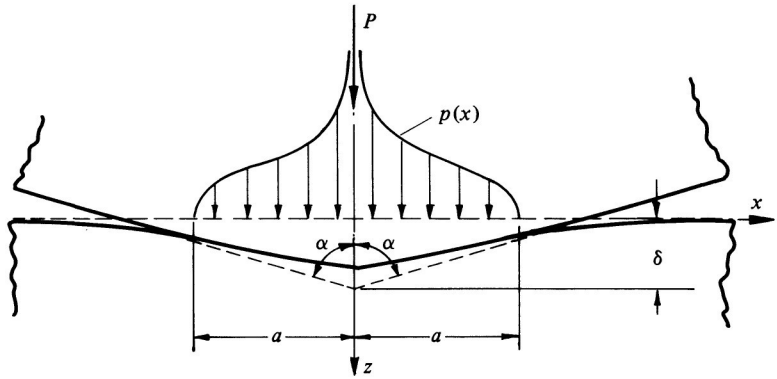

(*a*)

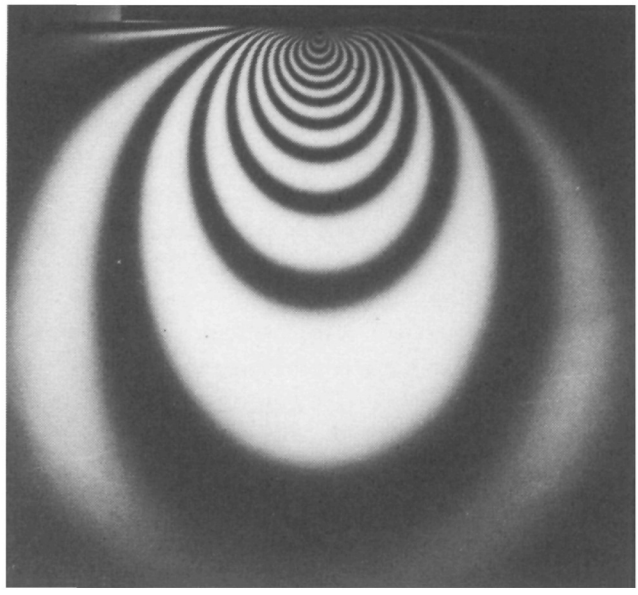

(*b*)

https://doi.org/10.1017/CBO9781139171731.006 Published online by Cambridge University Press

Thus

$$\bar{u}'_{z1} + \bar{u}'_{z2} = -(\text{sign } x) \cot \alpha \tag{5.6}$$

where (sign x) = +1 or −1 when x is +ve or −ve respectively. Neglecting friction, the normal pressure acting at the interface is found by substituting in equation (2.25*b*) to give

$$\frac{2}{\pi E^*} \int_{-a}^{a} \frac{p(s)}{x - s} \, \mathrm{d}s = (\text{sign } x) \cot \alpha \tag{5.7}$$

This is an integral equation for $p(x)$ of the type (2.39) with the general solution (2.41).

Now

$$\int_{-a}^{a} \frac{(a^2 - s^2)^{1/2} (\text{sign } s) \, \mathrm{d}s}{x - s} = \int_{0}^{a} \frac{(a^2 - s^2)^{1/2} \, \mathrm{d}s}{x - s} - \int_{-a}^{0} \frac{(a^2 - s^2)^{1/2} \, \mathrm{d}s}{x - s}$$

$$= \int_{0}^{a} (a^2 - s^2)^{1/2} \left\{ \frac{1}{x - s} - \frac{1}{x + s} \right\} \mathrm{d}s = 2 \int_{0}^{a} \frac{(a^2 - s^2)^{1/2} s \, \mathrm{d}s}{x^2 - s^2}$$

$$= 2a - (a^2 - s^2)^{1/2} \ln \left\{ \frac{a + (a^2 - x^2)^{1/2}}{a - (a^2 - x^2)^{1/2}} \right\} \tag{5.8}$$

Substituting in (2.41) and using (2.42), we get

$$p(x) = \frac{E^* \cot \alpha}{2\pi} \left[\frac{2a}{(a^2 - x^2)^{1/2}} - \ln \left\{ \frac{a + (a^2 - x^2)^{1/2}}{a - (a^2 - x^2)^{1/2}} \right\} \right] + \frac{P}{\pi (a^2 - x^2)^{1/2}} \tag{5.9}$$

If the smooth faces of the wedge extend beyond the edges of the contact the pressure must fall to zero at the edges to avoid tension or interference outside the contact, whence

$$P = aE^* \cot \alpha \tag{5.10}$$

The pressure distribution is then

$$p(x) = \frac{E^* \cot \alpha}{2\pi} \ln \left\{ \frac{a + (a^2 - x^2)^{1/2}}{a - (a^2 - x^2)^{1/2}} \right\} = \frac{E^* \cot \alpha}{\pi} \cosh^{-1}(a/x) \tag{5.11}$$

This pressure distribution is plotted in Fig. 5.2(*a*); it rises to an infinite value at the apex to the wedge. It would appear that the discontinuity in slope of the profiles within the contact region leads to a logarithmic singularity in pressure. Although the pressure is infinite at the apex of the wedge the principal shear stress in the x–z plane is not so. The stress components within the solids due to the pressure distribution (5.11) may be calculated using equation (2.23). Along

https://doi.org/10.1017/CBO9781139171731.006 Published online by Cambridge University Press

the z-axis, where σ_x and σ_z are principal stresses it turns out that

$$\tau_1 = \tfrac{1}{2}|\sigma_x - \sigma_z| = (E^*a/\pi)\cot\alpha\,(a^2 + z^2)^{-1/2} \tag{5.12}$$

which has a finite maximum value beneath the apex:

$$(\tau_1)_{\max} = (E^*/\pi)\cot\alpha$$

The indentation of a flat surface by a blunt cone gives similar results. Love (1939) used the classical approach outlined in §3.1 to find the appropriate potential function. He showed that the pressure on the face of the cone is given by

$$p(r) = \tfrac{1}{2}E^*\cot\alpha\cosh^{-1}(a/r) \tag{5.13}$$

and the total force

$$P = \tfrac{1}{2}\pi a^2 E^*\cot\alpha \tag{5.14}$$

Sneddon (1948) used the integral transform technique to obtain the same result and to evaluate all the components of stress within the solid. The tractions at the surface of a cone which adheres to the contacting solid have been found by Spence (1968).

The distribution of pressure on the cone is similar to that on the wedge: it rises to a theoretically infinite value at the apex. At that point the tangential stress in the surface is given by

$$\sigma_r = \sigma_\theta = -\tfrac{1}{2}(1 + 2\nu)p_0$$

which is also infinite. The special case of an incompressible material ($\nu = 0.5$) is noteworthy. By considering the surface stresses we find an infinite hydrostatic pressure exists at the apex. By considering the variations in stress along the z-axis, we find that the principal shear stress is given by

$$\tau_1 = \tfrac{1}{2}|\sigma_r - \sigma_z| = \tfrac{1}{2}E^*a^2\cot\alpha\,(a^2 + z^2)^{-1}$$

which has a maximum yet finite value $\frac{1}{2}E^*\cot\alpha$ at the apex. The state of stress at the apex therefore comprises a finite shear stress in a radial plane superposed on an infinite hydrostatic pressure. Contours of τ_1 beneath the wedge are shown by the photo-elastic fringes in Fig. 5.2(b).

5.3 Conforming surfaces

In the previous chapter smooth non-conforming surfaces in contact were defined: the initial separation between such surfaces in the contact region can be represented to an adequate approximation by a second-order polynomial. Non-conforming surfaces can therefore be characterised completely by their radii of curvature at the point of first contact. However when the undeformed profiles conform rather closely to each other a different description of their initial separation may be necessary. Conforming surfaces in contact frequently

depart in another way from the conditions in which the Hertz theory applies. Under the application of load the size of the contact area grows rapidly and may become comparable with the significant dimensions of the contacting bodies themselves. A pin in a hole with a small clearance is an obvious case in point. When the arc of contact occupies an appreciable fraction of the circumference of the hole neither the pin nor the hole can be regarded as an elastic half-space so that the Hertz treatment is invalid.

We will consider first the contact of bodies whose profiles in the contact region cannot be adequately represented by a second-order polynomial but, nevertheless, can still be regarded as half-spaces for the purpose of calculating elastic deformations and stresses.

The profiles are represented by a polynomial to the required degree of approximation. Thus for a two-dimensional contact (assuming symmetry about the point of first contact) we can express the initial separation by

$$h = z_1 + z_2 = A_1 x^2 + A_2 x^4 + \cdots + A_n x^{2n} + \cdots \tag{5.15}$$

and for a contact with axial symmetry

$$h = A_1 r^2 + A_2 r^4 + \cdots + A_n r^{2n} \tag{5.16}$$

Substituting (5.15) or (5.16) in equation (4.6) gives the condition which has to be satisfied by the normal displacements of each surface within the contact region. Steuermann (1939) has found the distributions of pressure $p_n(x)$ and $p_n(r)$ for profiles having the form $A_n x^{2n}$ and $A_n r^{2n}$ respectively. In the two-dimensional case we can use equations (2.47) and (2.48). Taking the index n as defined in (5.15) and allowing for the elasticity of both surfaces, equation (2.48) for the contact pressure becomes

$$p_n(x) = \frac{P_n}{\pi(a^2 - x^2)^{1/2}} - \frac{E^* n A_n a^{2n}}{(a^2 - x^2)^{1/2}} \left\{ \left(\frac{x}{a}\right)^{2n} - \tfrac{1}{2}\left(\frac{x}{a}\right)^{2n-2} - \frac{1 \cdot 3 \ldots (2n-3)}{2 \cdot 4 \ldots 2n} \right\} \tag{5.17}$$

If the profiles are smooth and continuous there cannot be an infinite pressure at $x = \pm a$, from which it follows that

$$P_n = n\pi E^* A_n a^{2n} \frac{1 \cdot 3 \ldots (2n-1)}{2 \cdot 4 \ldots 2n} \tag{5.18}$$

and

$$p_n(x) = nE^* A_n a^{2n-2} \left\{ \left(\frac{x}{a}\right)^{2n-2} + \tfrac{1}{2}\left(\frac{x}{a}\right)^{2n-4} + \cdots + \frac{1 \cdot 3 \ldots (2n-3)}{2 \cdot 4 \ldots (2n-2)} \right\} (a^2 - x^2)^{1/2} \tag{5.19}$$

https://doi.org/10.1017/CBO9781139171731.006 Published online by Cambridge University Press

The second-order profiles assumed in the Hertz theory correspond to $n = 1$, in which case equations (5.17) and (5.19) reduce to (4.43) and (4.44) respectively. For higher values of n the pressure has its maximum values away from the centre of the contact. As $n \to \infty$ the configuration approaches that of two flat surfaces which make contact over a strip $|x| \leqslant a$, and are separated by thin gaps or cracks on either side. The pressure distribution in this case approaches that for a flat rigid punch in which the pressure is infinite at the edges. When the profiles can be represented by a single term in equation (5.15) the size of the contact strip is related to the load by equation (5.18). With a more general profile, the pressure distribution and total load are given by the superposition of expressions such as (5.18) and (5.19).

In the axi-symmetric case Steuermann finds the equivalent expressions:

$$P_n = \frac{4A_n E^* n a^{2n+1}}{(2n+1)} \frac{2 \cdot 4 \ldots 2n}{1 \cdot 3 \ldots (2n-1)} \tag{5.20}$$

$$p_n(r) = \frac{nA_n E^* a^{2n-2}}{\pi} \left\{ \frac{2 \cdot 4 \ldots 2n}{1 \cdot 4 \ldots (2n-1)} \right\}^2 \left\{ \left(\frac{r}{a}\right)^{2n-2} + \tfrac{1}{2}\left(\frac{r}{a}\right)^{2n-4} + \cdots + \frac{1 \cdot 3 \ldots (2n-3)}{2 \cdot 4 \ldots (2n-2)} \right\} (a^2 - r^2)^{1/2} \tag{5.21}$$

The compression can also be found in this case:

$$\delta = \frac{2 \cdot 4 \ldots 2n}{1 \cdot 3 \ldots (2n-1)} A_n a^{2n} \tag{5.22}$$

The two examples given above were capable of analytical solution because the shape of the area of contact was known in advance. For more general profiles this shape is not known; only for second-order surfaces will it be an ellipse. Some idea of the shape may be obtained from contours of equal separation before deformation, but it cannot be assumed that this shape will be maintained after deformation. Numerical methods of finding the contact stresses between conforming bodies of arbitrary profile are described in §9.

We turn now to two problems of contact between conforming solids which cannot be represented by half-spaces: (*a*) the two-dimensional contact of a pin in a hole in an infinite plate and (*b*) the contact of a sphere with a conforming spherical cavity. The geometry for a pin and hole is shown in Fig. 5.3. The difference in radii ΔR $(= R_2 - R_1)$ is small compared with either R_1 or R_2. The external load P is applied to the pin effectively at its centre C and causes C to displace by δ; the reaction is taken by a uniform stress in the plate at a large distance from the hole. The deformation in the contact region is shown in Fig. 5.3(*b*). Points on the two surfaces S_1 and S_2 which come into contact on the interface at S experience both radial and tangential elastic displacements $\bar{u}_r$ and

https://doi.org/10.1017/CBO9781139171731.006 Published online by Cambridge University Press

$\bar{u}_\theta$. Since ΔR and δ are both small compared with R_1 and R_2,

$$(R_2 + \bar{u}_{r2}) - (R_1 + \bar{u}_{r1}) = (\Delta R + \delta)\cos\phi \tag{5.23}$$

i.e.

$$\bar{u}_{r2} - \bar{u}_{r1} = \delta\cos\phi - \Delta R\,(1 - \cos\phi) \tag{5.24}$$

When the contact arc subtends an angle $\pm\alpha$ which is not small, expression (5.24) differs significantly from the Hertz approximation given by equation (4.37). It is now required to find the distribution of normal pressure (neglecting friction) which, when acting over the arc $\pm\alpha$, produces displacements in the surface of the pin and hole which satisfy (5.24) in the interval $-\alpha < \phi < \alpha$. This problem has been studied in detail by Persson (1964) who has used stress functions appropriate to a circular disc and to a circular hole in an infinite plate to obtain the complete stress field for both pin and hole.

Pressure distributions for different values of α are shown in Fig. 5.4(*a*). The variation of the contact arc α with load P is shown in Fig. 5.4(*b*), both for a pin with clearance (ΔR positive) and a pin with interference (ΔR negative). With small loads or large clearance the relationship approaches that of Hertz (eq. (4.42)). The relationship given by Steuermann's theory is also shown. Here the gap between the pin and the hole has been represented by a power series and the contact pressure and load calculated from equations (5.17)–(5.19). The result, though better than that of Hertz by the inclusion of higher terms in the description of the profile, is still in error through Steuermann's assumption that both solids can be regarded as elastic half-spaces.

The analogous problem of a frictionless sphere in a conforming cavity has been analysed by Goodman & Keer (1965) using methods appropriate to spherical bodies. They find that the contact is up to 25% stiffer in compression than would be predicted by the Hertz theory.

Fig. 5.3. Pin in a conforming hole.

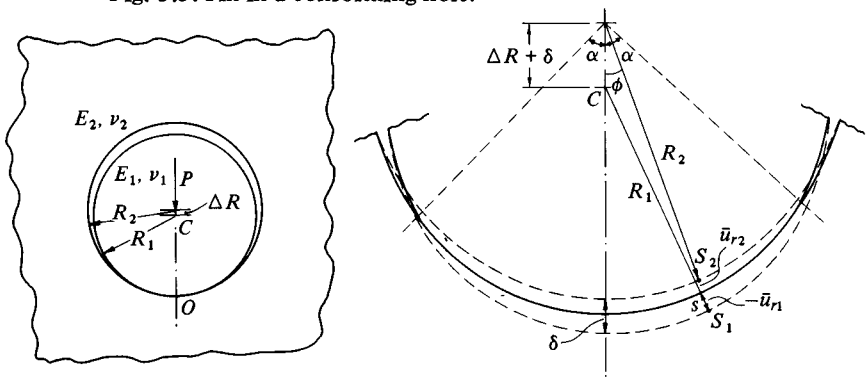

(*a*) (*b*)

https://doi.org/10.1017/CBO9781139171731.006 Published online by Cambridge University Press

Fig. 5.4. Pin in a conforming hole: $E_1 = E_2 = E$, $\nu_1 = \nu_2 = 0.30$. (*a*) contact pressure; (*b*) contact arc. (From Persson, 1964.)

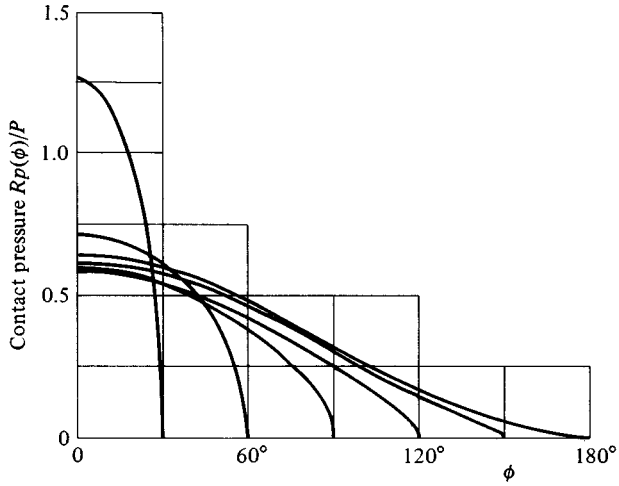

(*a*)

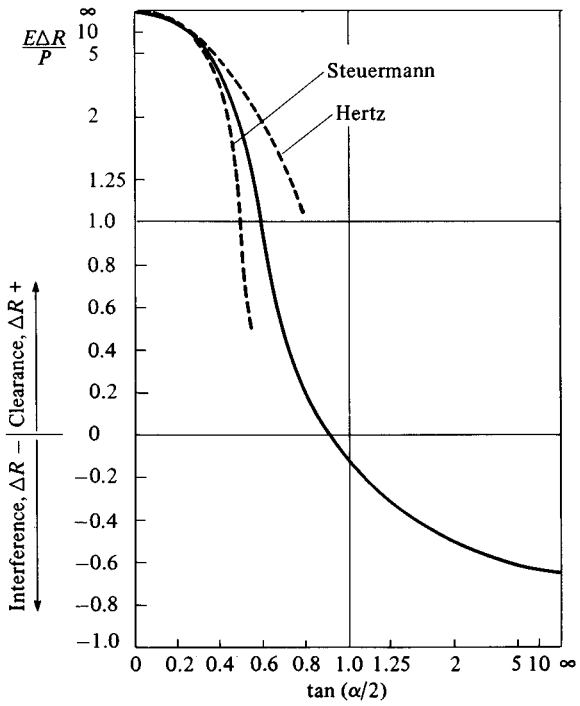

(*b*)

https://doi.org/10.1017/CBO9781139171731.006 Published online by Cambridge University Press

5.4 Influence of interfacial friction

Friction at the interface of two non-conforming bodies brought into normal contact plays a part only if the elastic constants of the two materials are different. The mutual contact pressure produces tangential displacements at the interface as well as normal compression (see equation (3.41*b*) for spheres in contact). If the materials of the two solids are dissimilar, the tangential displacements will, in general, be different so that slip will take place. Such slip will be opposed by friction and may, to some extent, be prevented. We might expect therefore a central region where the surfaces stick together and regions of slip towards the edge of the contact. If the coefficient of limiting friction were sufficiently high slip might be prevented entirely.

In the first studies of this problem (Mossakovski, 1954, 1963; Goodman, 1962) the build-up of tangential traction at the interface was developed incrementally for a growth in contact size from a to $a + \mathrm{d}a$. However, as Spence (1968) pointed out, under appropriate conditions the stress field is self-similar at all stages of loading so that the solution may be obtained directly without recourse to an incremental technique.

In setting up the boundary conditions of the problem we start by assuming that where there is slip the tangential traction q is related to the normal pressure p by

$$|q| = \mu p \tag{5.25}$$

where μ is a constant coefficient of friction. The direction of q opposes the direction of slip. In a two-dimensional contact q acts in a direction parallel to the x-axis, inwards on one surface and outwards on the other. In an axi-symmetrical contact the slip, and hence q, must be radial and axi-symmetrical. For non-conforming surfaces having quadratic profiles we deduced in §4.1 (eq. (4.11)) that the magnitude of the stress and strain at any point increases in proportion to the contact size a. In consequence of (5.25) the stresses and strains due to the shear traction also increase in proportion to a, and the boundary between the slipped and adhered regions will be located at a constant fraction of a. In this way self-similarity of the stress field is maintained at all stages of loading.

As the load is increased and the contact size grows, mating points on the two surfaces, which initially lie outside the adhesion zone, undergo different tangential displacements. After they are enveloped by the adhesion zone, they cease to experience any further relative displacement. Such points will then maintain the relative tangential displacement $(\bar{u}_{x1} - \bar{u}_{x2})$ and relative strain $(\partial\bar{u}_{x1}/\partial x - \partial\bar{u}_{x2}/\partial x)$ which they had acquired up to that instant. Now the magnitude of the strain grows in direct proportion to a so that, for two contacting points lying in the adhesion zone at a distance x from the centre, we can write

https://doi.org/10.1017/CBO9781139171731.006 Published online by Cambridge University Press

$$\frac{\partial \bar{u}_{x1}}{\partial x} - \frac{\partial \bar{u}_{x2}}{\partial x} = C|x| \tag{5.26}$$

where C is a constant to be determined.

Consider first the contact of two parallel cylinders. At a particular stage in loading the contact width is $2a$ and we will assume that friction prevents slip over a central region of width $2c$. A symmetrical normal pressure $p(x)$ and an anti-symmetrical tangential traction $q(x)$ act at the interface. The normal displacement gradients within the whole contact region are given by equation (4.39). Substituting into equation (2.25*b*) and remembering that the tractions on each surface are equal and opposite, we find

$$\int_{-a}^{a} \frac{p(s)}{x-s}\,\mathrm{d}s - \pi\beta q(x) = \pi E^* x/2R, \quad -a \leqslant x \leqslant a \tag{5.27}$$

where $1/R = 1/R_1 + 1/R_2$ and the constant β is a measure of the difference in elastic constants of the two materials defined by equation (5.3). In the adhesion region, substituting (2.25*a*) into the condition of no-slip given by (5.26) gives

$$\pi\beta p(x) + \int_{-a}^{a} \frac{q(s)\,\mathrm{d}s}{x-s} = -\tfrac{1}{2}\pi E^* C|x|, \quad |x| \leqslant c \tag{5.28}$$

Also for no-slip

$$|q| \leqslant \mu p \tag{5.29}$$

In the slip regions

$$q = \pm\mu p, \quad c < |x| < a \tag{5.30}$$

where the sign q is determined by the direction of slip. If equations (5.27) to (5.30) are divided by the contact size a they are transformed into equations for (p/a), (q/a) which are independent of the actual value of a, thereby confirming the previous argument that similarity of the stress field is maintained during loading.

As a first step to solving equations (5.27) and (5.28) for the tractions $p(x)$ and $q(x)$ we simplify the problem by assuming that there is no slip throughout the contact area. Equation (5.28) then applies over the interval ($|x| \leqslant a$) and, together with (5.27), provides dual integral equations for $p(x)$ and $q(x)$ of the type discussed in §2.7, having boundary conditions of class III. A further simplification results from neglecting the influence of the shear traction upon the normal pressure, i.e. by neglecting the second term on the left-hand side of (5.27). The equations are now uncoupled. The pressure distribution is given by the Hertz theory (equation (4.44)) and equation (5.28) for the tangential traction may be written

$$\int_{-a}^{a} \frac{q(s)\,\mathrm{d}s}{s-x} = -\pi\beta p_0(1 - x^2/a^2)^{1/2} - \tfrac{1}{2}\pi E^* C|x| \tag{5.31}$$

https://doi.org/10.1017/CBO9781139171731.006 Published online by Cambridge University Press

This is an integral equation of the type (2.39) having a general solution given by (2.41).

It is convenient to imagine the traction $q(x)$ as being made up of two components: $q'(x)$ and $q''(x)$, which satisfy (5.31) with each of the terms on the right-hand side taken in turn. Thus $q'(x)$ is the tangential traction necessary to cancel the difference in tangential displacements arising from the normal pressure, and $q''(x)$ is the traction necessary to produce the additional displacements, proportion to $|x|$, which are necessary to satisfy the no-slip condition. Substituting into (2.41) and integrating we find

$$q'(x) = 2\beta\frac{p_0}{\pi}\left[\frac{x}{(a^2-x^2)^{1/2}} + \frac{1}{2a}(a^2-x^2)^{1/2}\ln\left|\frac{a+x}{a-x}\right|\right] \tag{5.32}$$

and

$$q''(x) = \frac{CE^*}{2\pi}\left[-\frac{2x}{(a^2-x^2)^{1/2}} + x\ln\left\{\frac{a+(a^2-x^2)^{1/2}}{a-(a^2-x^2)^{1/2}}\right\}\right] \tag{5.33}$$

The constant C is determined by the fact that the traction should fall to zero at the edges of the contact. Therefore the term $(a^2-x^2)^{-1/2}$ must vanish when $q'(x)$ and $q''(x)$ are added, whereupon

$$C = 2\beta p_0/E^*a$$

and

$$q(x) = \frac{\beta p_0}{\pi a}\left[(a^2-x^2)^{1/2}\ln\left|\frac{a+x}{a-x}\right| + x\ln\left\{\frac{a+(a^2-x^2)^{1/2}}{a-(a^2-x^2)^{1/2}}\right\}\right] \tag{5.34}$$

If the ratio of $q(x)$ to $p(x)$ is examined we find that it rises to infinity at the edges of the contact, which shows that some slip is inevitable. The realistic circumstances in which slip takes place on each side of a central no-slip zone of width $2c$ have been studied by Spence (1975).

On similarity grounds Spence has shown that, for the same elastic constants and coefficient of friction, the extent of the slip region is the same for any indenter having the profile $z = Ax^n$ and is equal to that for a flat-ended punch. The value of c is therefore given by equation (2.73) in which $(1-2\nu)/(1-\nu)$ is replaced by 2β to take into account the elasticity of both bodies. This relationship is plotted in Fig. 5.5 (curve A). The traction has been evaluated by Spence and is shown in Fig. 5.6, for $\mu/\beta = 0.99$, which gives $c = 0.7a$.

The contact of dissimilar spheres without slip has been analysed by Goodman (1962) on the basis of neglecting the influence of tangential traction on normal pressure. If the traction is again separated into the two components: to cancel the tangential displacements due to normal pressure requires

Fig. 5.5. Normal contact of dissimilar solids: the extent of the slip region: curve A – line contact, eq. (2.73); curve B – axi-symmetric point contact, eq. (5.38).

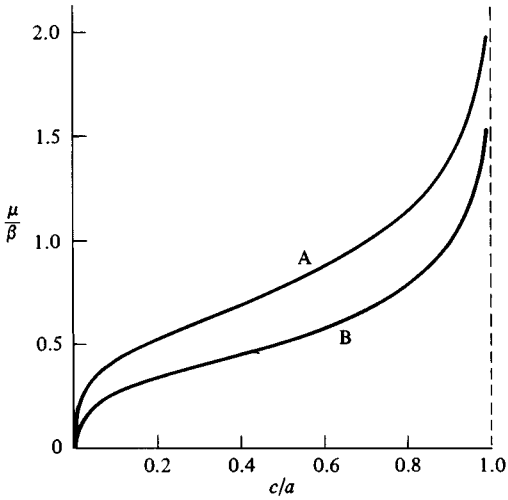

Fig. 5.6. Tangential tractions at contact of dissimilar solids. (*a*) Line contact: A – no slip, eq. (5.34); B – partial slip, $\mu/\beta = 0.99$. (*b*) Point contact: C – no slip, eq. (5.37); D – partial slip, $\mu/\beta = 0.66$. Broken lines – $\mu p/\beta p_0$.

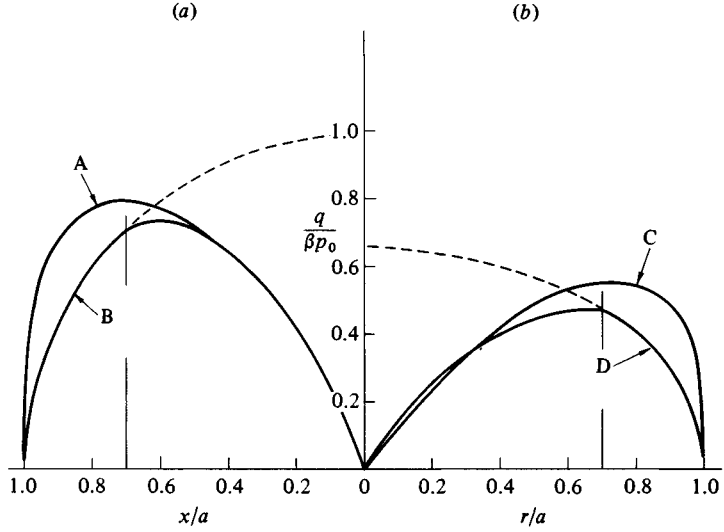

https://doi.org/10.1017/CBO9781139171731.006 Published online by Cambridge University Press

$$q'(r) = \frac{\beta p_0}{\pi}\frac{1}{r}\left[a^2(a^2-r^2)^{-1/2} - 2(a^2-r^2)^{1/2} + \int_r^a \frac{t^2}{(t^2-r^2)^{1/2}} \ln\left|\frac{t+r}{t-r}\right| dt\right] \tag{5.35}$$

and to satisfy the no-slip condition (5.26) requires

$$q''(r) = \frac{3CE^*}{8}\left[-r(a^2-r^2)^{-1/2} + \frac{r}{a}\ln\left\{\frac{a+(a^2-r^2)^{1/2}}{r}\right\}\right] \tag{5.36}$$

The unknown constant C is again determined by the condition that the resultant traction should be zero at $r = a$, whereupon

$$q(r) = \frac{\beta p_0}{\pi}\left[-\frac{1}{r}(a^2-r^2)^{1/2} + \frac{r}{a}\ln\left\{\frac{a+(a^2-r^2)^{1/2}}{r}\right\} + \frac{2}{ra}\int_r^a \frac{t^2}{(t^2-r^2)^{1/2}} \ln\left|\frac{t+r}{t-r}\right| dt\right] \tag{5.37}$$

This traction is plotted in Fig. 5.6. The ratio $q(r)/p(r)$ is again infinite at $r = a$, so that some slip must occur. The extent of the slip region in monotonic loading is the same as for a rigid flat punch, and is given by

$$\frac{a}{2c}\ln\left(\frac{a+c}{a-c}\right) = \frac{\beta}{\mu}\mathbf{K}'(c/a) \tag{5.38}$$

where $\mathbf{K}'(c/a)$ is the complete elliptical integral of argument $(1-c^2/a^2)^{1/2}$. This relationship is also shown in Fig. 5.5 (curve B), and the traction when $c = 0.7a$ is plotted in Fig. 5.6. As the coefficient of friction is decreased the no-slip circle shrinks towards the central point and the traction approaches $\mu p(r)$.

Complete solutions to the problem which include the influence of tangential traction on the pressure have been obtained by Mossakovski (1963) and Spence (1968, 1975). They show that, depending upon the value of β, friction can increase the total load required to produce a contact of given size by at most 5% compared with Hertz.

Distributions of frictional traction for line contact and axi-symmetrical point contact are plotted in Fig. 5.6. They act outwards on the more deformable surface and inwards on the more rigid one. Without slip the magnitude of the traction is proportional to the parameter β which characterises the difference in elastic properties of the materials. Clearly β vanishes not only when the materials are identical but also when they are both incompressible ($\nu = 0.5$).

In these cases frictional tractions are absent and the Hertz solution applies. Some values of β for typical pairs of materials are given in Table 5.1. The maximum possible value of β is 0.5 and practical values rarely exceed 0.2. Thus the frictional traction is much smaller than the normal pressure and its influence on the internal stresses in not great. It does have an important effect, however, on the tangential stress $\bar{\sigma}_x$ or $\bar{\sigma}_r$ at the surface just outside the contact area. In the case of line contact, without slip, the traction of equation (5.34) gives rise to stresses at the edge of contact given by

$$\bar{\sigma}_x(-a) = \bar{\sigma}_x(a) = -2\beta p_0 \tag{5.39}$$

compressive on the compliant surface and tensile on the rigid one. Slip will have the effect of reducing this stress. If slip were complete, so that $|q| = \mu p$ everywhere

$$\bar{\sigma}_x(-a) = \bar{\sigma}_x(a) = -(4/\pi)\mu p_0 \tag{5.40}$$

In reality slip will only be partial and there will be a no-slip zone in the centre of width $2c$. However equation (5.40) is a good approximation provided $c/a < 0.7$, i.e. when $\mu/\beta < 1.0$.

For the axi-symmetric case the radial stress in the surface may be calculated using equation (3.103c). With no slip the traction of equation (5.37) gives rise to a radial stress in the surface at $r = a$ given by

$$\bar{\sigma}_r(a) = -1.515(1 - 0.16\nu)\beta p_0 \tag{5.41}$$

If, on the other hand, complete slip takes place

$$\bar{\sigma}_r(a) = -1.185(1 - 0.23\nu)\mu p_0 \tag{5.42}$$

Again equation (5.42) is a good approximation for partial slip provided $c/a < 0.7$, when $\mu/\beta < 0.66$. In the axi-symmetric case the normal pressure itself gives rise to a radial tension outside the contact circle which has a maximum value $\frac{1}{3}(1 - 2\nu)p_0$ at $r = a$ and decreases as r^{-2} (eq. (3.44)). On the more compliant surface (β + ve) the compressive stress produced by the frictional traction attenuates the tension coming from the normal pressure and has the effect of pushing the location of the maximum tension to a radius somewhat greater than a. On the more rigid surface (β − ve) the radial stress due to friction is tensile and adds to that due to pressure to give a maximum tension at $r = a$. Johnson, O'Connor & Woodward (1973) have investigated this effect and have shown that it influences the resistance of brittle materials to Hertzian fracture when the material of the indenter is different from that of the specimen.

The frictional traction which develops when the load is reduced is also of interest in view of the observation that ring cracks frequently occur during unloading. Some appreciation of this behaviour may be obtained from Turner's analysis (1979) of unloading a flat-ended punch.

5.5 Adhesion between elastic bodies

So far in this book we have taken it for granted that, while a mutual pressure is exerted at the interface between two bodies in contact, no tensile traction can be sustained. This assumption accords with common experience that, in the absence of a specific adhesive, the contact area between non-conforming elastic solids falls to zero when the load is removed and that no tensile force is required to separate them. On the other hand, a physicist describing the interaction between the ideal surfaces of two solids would tell a different story (see, for example, Tabor, 1975). As a result of the competing forces of attraction and repulsion between individual atoms or molecules in both bodies, two ideally flat solid surfaces will have an equilibrium separation z_0; at a separation less than z_0 they will repel each other and at a separation greater than z_0 they will attract. The variation of force per unit area as a function of separation z is usually represented by a law of the form

$$p(z) = -Az^{-n} + Bz^{-m}, \quad m > n \tag{5.43}$$

as shown in Fig. 5.7 where the pressure (repulsion) is taken to be positive. In these circumstances it is clear that a tensile force - the 'force of adhesion' - has to be exerted to separate the surfaces. The magnitude of the maximum tensile traction is large, but the effective range of action is very small. In view of the difficulty in measuring surface forces directly, it is usual to measure the work 2γ required to separate the surfaces from $z = z_0$ to $z = \infty$ and to ascribe a *surface energy* γ to each newly created free surface. If the solids are dissimilar, the work to separate the surfaces becomes $\gamma_1 + \gamma_2 - 2\gamma_{12}$ where γ_1 and γ_2 are the intrinsic surface energies of the two solids and γ_{12} is the energy of the interface.

The reason why this expected adhesion between solids is not usually observed, even when great care is taken to remove contaminant films, lies in the inevitable

Fig. 5.7. Force–separation curve and surface energy for ideal surfaces, eq. (5.43).

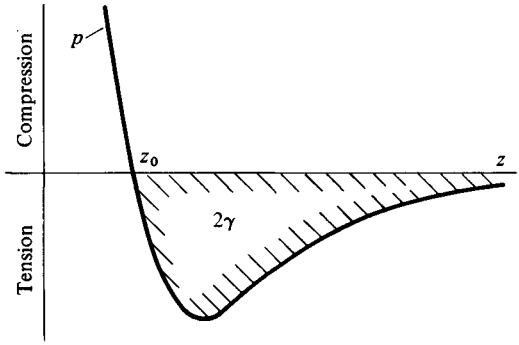

https://doi.org/10.1017/CBO9781139171731.006 Published online by Cambridge University Press

roughness of real surfaces, whose asperity heights are large compared with the range of action of the adhesive forces. The real area of contact, which occurs at the crests of the high spots, is much smaller than the apparent area (see Chapter 13). Adhesive junctions formed between the lower asperities on loading are elbowed apart on unloading by the compression between the higher asperities. In this way adhesion developed at the points of real contact is progressively broken down. Exceptions to this state of affairs arise with (*a*) cleaved mica which can be prepared with an atomically smooth surface and (*b*) low modulus solids such as gelatine or rubber which can mould themselves to accommodate a modest amount of surface roughness. In these circumstances the real area of contact is identical with the apparent area.

To study the effect of adhesive forces in the absence of surface roughness we shall consider two non-conforming axi-symmetric solids which make contact over a circular area, of radius a. Frictional tractions of the sort discussed in the previous section will be ignored (see Johnson *et al.*, 1971; and Johnson, 1976). The normal elastic displacement in the contact circle produced by the normal traction must satisfy equation (4.17), i.e.

$$\bar{u}_{z1} + \bar{u}_{z2} = \delta - r^2/2R$$

We found in §4.2(*a*) that this condition was satisfied by a pressure distribution of the form

$$p(r) = p_0(1 - r^2/a^2)^{1/2} + p_0'(1 - r^2/a^2)^{-1/2} \tag{5.44}$$

where $p_0 = 2aE^*/\pi R$. A positive value of p_0' was rejected since an infinite pressure at $r = a$ implied interference between the two surfaces outside the contact area: a negative value of p_0' was rejected on the grounds that tension could not be sustained. In the presence of adhesive (attractive) forces, however, we cannot exclude the possibility of a negative p_0'. By considering the work done in compression by the pressure of (5.44), the elastic strain energy stored in the two bodies is easily shown to be

$$U_E = \frac{\pi^2 a^3}{E^*}\left(\tfrac{2}{15}p_0^2 + \tfrac{2}{3}p_0 p_0' + p_0'^2\right) \tag{5.45}$$

The total compression is found from equations (3.36) and (4.20) to be

$$\delta = (\pi a/2E^*)(p_0 + 2p_0') \tag{5.46}$$

We now consider the variation in strain energy U_E with contact radius a, keeping the overall relative displacement of the two bodies δ constant. With p_0 as specified above we find

$$\left[\frac{\partial U_E}{\partial a}\right]_\delta = \frac{\pi^2 a^2}{E^*} p_0'^2 \tag{5.47}$$

https://doi.org/10.1017/CBO9781139171731.006 Published online by Cambridge University Press

Since δ is kept constant no external work is done, so that for equilibrium we would expect $\partial U_E/\partial a$ to vanish, giving $p_0' = 0$, as indeed it is in the Hertz theory.

In the present problem, adhesive forces introduce a surface energy U_S which is decreased when the surfaces come into intimate contact and increased when they separate. Therefore we can write

$$U_S = -2\gamma\pi a^2$$

where γ is the surface energy per unit area of each surface. The total free energy of the system is now

$$U_T = U_E + U_S$$

For equilibrium $[\partial U_T/\partial a]_\delta$ vanishes giving

$$\frac{\pi^2 a^2}{E^*} p_0'^2 = -\frac{\partial U_S}{\partial a} = 4\pi\gamma a$$

i.e.

$$p_0' = -(4\gamma E^*/\pi a)^{1/2} \tag{5.48}$$

where the minus sign is chosen since compressive stresses at $r = a$ have been excluded. The net contact force is given by

$$P = \int_0^a 2\pi r p(r)\, dr = (\tfrac{2}{3}p_0 + 2p_0')\pi a^2$$

Substituting for p_0 and p_0' and rearranging give a relationship between a and P:

$$\left(P - \frac{4E^* a^3}{3R}\right)^2 = 16\pi\gamma E^* a^3 \tag{5.49}$$

This relationship is plotted in Fig. 5.8 where it is compared with experimental measurements using gelatine spheres in contact with perspex. When the bodies are loaded by a compressive (positive) force the adhesive forces pull the surfaces into contact over an area which exceeds that given by the Hertz theory. Reducing the load to zero leaves the surfaces adhering together with a radius given by point C in Fig. 5.8. The application of a tensile (negative) load causes the contact radius to shrink further. At point B, when

$$P = -P_c = -3\pi\gamma R \tag{5.50}$$

and

$$a = a_c = (9\gamma R^2/4E^*)^{1/3} \tag{5.51}$$

the situation becomes unstable and the surfaces separate. Thus P_c given by equation (5.50) is the 'force of adhesion'. If, instead of controlling the load, we control the relative displacement δ between the solids, the adhesive contact

is stable down to point A in Fig. 5.8 ($P = -5P_c/9, a = a_c/3^{2/3}$). Beyond this point the adhesive junction breaks.

The traction distribution given by (5.44) and the shape of the deformed surface outside the contact (from equations (3.38) and (3.42*a*)) are shown in Fig. 5.9 for an elastic sphere in contact with a rigid flat surface. There is an infinite tensile traction and the deformed profile meets the flat surface in a sharp corner at $r = a$. In reality the stress will not be infinite nor the corner perfectly sharp, but there will be some rounding of the corner until the surface traction is consistent with the force-separation law illustrated in Fig. 5.7. Provided that the elastic displacements are large compared with the effective range of action of the surface forces, the analysis outlined above will give a good measure of the influence of adhesion on the deformation of elastic bodies in contact. The idealisation is the same as that of a Griffith crack in linear elastic fracture mechanics. Indeed the gap just outside the contact of two separating bodies may be thought of as an opening crack. Maugis *et al.* (1976, 1978) and also Greenwood & Johnson (1981) have made use of the 'stress intensity factor'

Fig. 5.8. Variation of contact radius with load, eq. (5.49), compared with measurements on gelatine spheres in contact with perspex. Radius R: circle – 24.5 mm, cross – 79 mm, square – 255 mm.

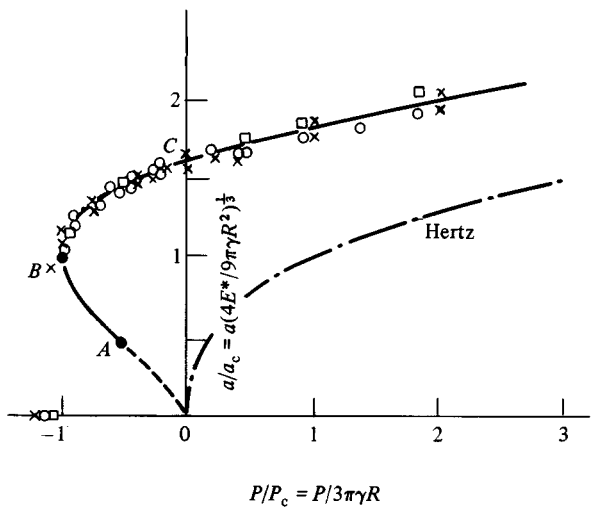

https://doi.org/10.1017/CBO9781139171731.006 Published online by Cambridge University Press

Fig. 5.9. Surface traction and deformation of an elastic sphere in contact with a rigid plane, solid line – with adhesion, eq. (5.44), broken line – without adhesion (Hertz).

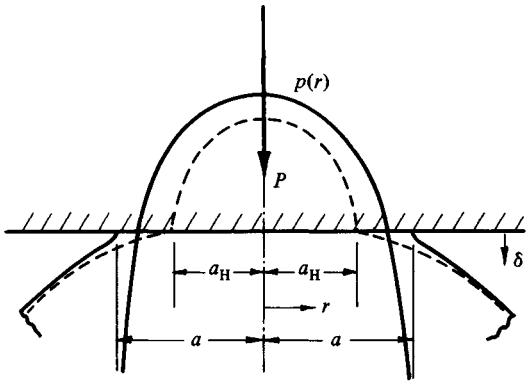

concept of fracture mechanics to analyse the adhesive contact of elastic and viscoelastic solids.

5.6 Contact of cylindrical bodies

The elastic compression of two-dimensional bodies in contact cannot be calculated solely from the contact stresses given by the Hertz theory. Some account must be taken of the shape and size of the bodies themselves and the way in which they are supported. In most practical circumstances such calculations are difficult to perform, which has resulted in a variety of approximate formulae for calculating the elastic compression of bodies in line contact such as gear teeth and roller bearings in line contact (Roark, 1965; Harris, 1966). However the compression of a long circular cylinder which is in non-conformal contact with two other surfaces along two generators located at opposite ends of a diameter can be analysed satisfactorily.

Such a cylinder is shown in cross-section in Fig. 5.10. The compressive load per unit axial length P gives rise to a Hertzian distribution of pressure at O_1

$$p = \frac{2P}{\pi a_1}(1 - x^2/a_1^2)^{1/2} \tag{5.52}$$

where the semi-contact-width is given by

$$a_1^2 = 4PR/\pi E_1^* \tag{5.53}$$

where E_1^* is the composite modulus of the roller and the contacting body.

https://doi.org/10.1017/CBO9781139171731.006 Published online by Cambridge University Press

The stress distribution in a cylinder due to diametrically opposed concentrated loads is given by Timoshenko & Goodier (1951) p. 107. It comprises the superposition of the stress fields due to two concentrated forces P acting on the plane boundaries of two half-spaces tangential to the cylinder at O_1 and O_2 (see eq. (2.14)), together with a uniform bi-axial tension:

$$\sigma_x = \sigma_z = P/\pi R \tag{5.54}$$

which frees the circular boundary of the cylinder from stress.

Since $a \ll R$ we can consider the cylinder in Fig. 5.10 as being subjected to a combination of diametrically opposed forces distributed according to (5.52). We now require the radial component of strain ϵ_z at a point A lying between O_1 and C on the axis of symmetry. The state of stress at A is made up of three contributions: (i) the stress due to the Hertzian distribution of pressure on the contact at O_1, given by equation (5.52); (ii) the stress due to the contact pressure at O_2, which, in view of the large distance of A from O_2, can be taken to be that due to a concentrated force P, given by equation (2.16); and (iii) the bi-axial tension given by (5.54). Adding these three contributions we obtain for

Fig. 5.10

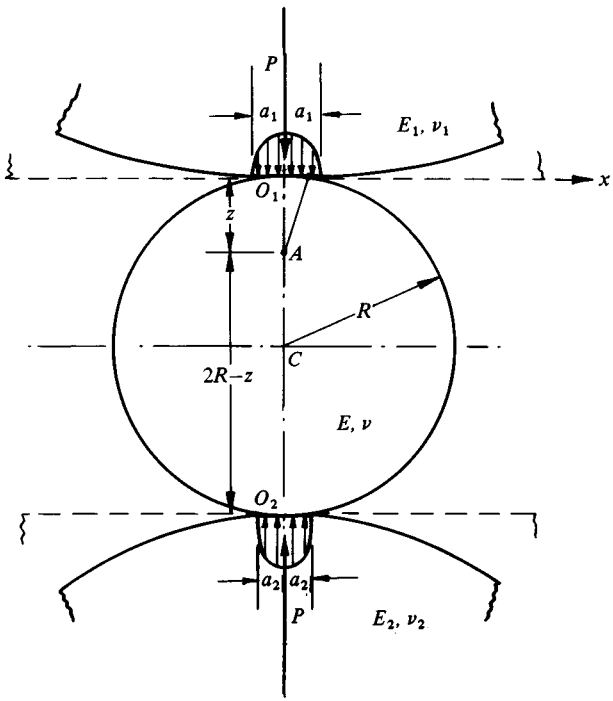

https://doi.org/10.1017/CBO9781139171731.006 Published online by Cambridge University Press

the stresses at A:

$$\sigma_x = \frac{P}{\pi}\left\{\frac{1}{R} - \frac{2(a_1^2 + 2z^2)}{a_1^2(a_1^2 + z^2)^{1/2}} + \frac{4z}{a_1^2}\right\} \tag{5.55a}$$

$$\sigma_z = \frac{P}{\pi}\left\{\frac{1}{R} - \frac{2}{2R - z} - \frac{2}{(a_1^2 + z^2)^{1/2}}\right\} \tag{5.55b}$$

In plane strain

$$\epsilon_z = \{(1 - \nu^2)/E\}\{\sigma_z - \sigma_x \nu/(1 - \nu)\}$$

The compression of the upper half of the cylinder O_1C is then found by integrating ϵ_z from $z = 0$ to $z = R$, where $a \ll R$, to give

$$\delta_1 = P\frac{(1 - \nu^2)}{\pi E}\{2 \ln (4R/a_1) - 1\} \tag{5.56}$$

A similar expression is obtained for the compression of the lower half of the cylinder so that the total compression of the diameter through the mid-points of the contact areas O_1O_2 is

$$\delta = 2P\frac{(1 - \nu^2)}{\pi E}\{\ln (4R/a_1) + \ln (4R/a_2) - 1\} \tag{5.57}$$†

For comparison we can calculate the compression of a half-space relative to a point at a depth d below the centre of a Hertzian contact pressure distribution, with the result:

$$\delta = P\frac{(1 - \nu^2)}{\pi E}\{2 \ln (2d/a) - \nu/(1 - \nu)\} \tag{5.58}$$

Taking $d = R$ the true compression of the half-cylinder (5.56) exceeds the compression based upon a half-space (5.58) by less than 10% within the practical range of loads.

When one of the contacting bodies roughly takes the form of a rectangular block of thickness t, then the compression of the block through its thickness may be obtained with reasonable approximation by putting $d = t$ in equation (5.58), provided that the thickness of the block is large compared with the contact width ($t \gg a$).

Another important feature of the contact of cylindrical bodies falls outside the scope of the Hertz theory. Real cylinders are of finite length and, although the contact stresses over the majority of the length of the cylinder are predicted accurately by the Hertz theory, significant deviations occur close to the ends.

† This expression differs from a much quoted result due to Föeppl (*Drang und Zwang*, vol. I, p. 319, 1924) on account of Föeppl's use of a *parabolic* contact pressure distribution.

https://doi.org/10.1017/CBO9781139171731.006 Published online by Cambridge University Press

In most circumstances there is a concentration of contact stress at the ends which makes the effect of practical importance. In the design of roller bearings, for example, the axial profile of the rollers is modified with a view to eliminating the stress concentration at the ends. The different possible end conditions which may arise when a uniform cylinder is in contact with another surface are shown diagrammatically in Fig. 5.11. In case (*a*) both surfaces come to an end at the same cross-sectional plane. On cross-sections away from the ends an axial compressive stress $\sigma_y = \nu(\sigma_x + \sigma_z)$ exists to maintain the condition of plane strain. At the free ends this compressive stress is relaxed, permitting the solids to expand slightly in the axial direction and thereby *reducing* the contact pressure at the end.

An estimate of the reduction in pressure at the end may be obtained by assuming that the end of the cylinder is in a state of *plane stress.* Equation (5.56) for the radial compression of the cylinder may be written

$$\delta = (a^2/2R)\{2 \ln (4R/a) - 1\} \tag{5.59}$$

which applies for both plane stress and plane strain. If the cylinder does not tilt, the compression δ is uniform along its length, so that the contact width a must also be approximately uniform right up to the end. Now in plane strain $a = 2p_0R(1-\nu^2)/E$ whereas in plane stress $a = 2p_0'R/E$. Hence the pressure at the end $p_0' \approx (1-\nu^2)p_0$.

In case (*b*) the roller has a square end but the mating surface extends beyond the end. In this case there is a sharp stress concentration at the end of the roller. The nature of the singularity can be assessed from the considerations discussed in §1. For example, with no friction and equal elastic moduli the contact pressure at a small distance y from the end ($y \ll a$) will vary as $y^{-0.23}$.

Case (*c*) is typical of a cylindrical bearing roller. The track surface extends beyond the end of the roller and the roller itself has a profile of radius r connecting the cylindrical body smoothly with the flat end. Provided r is appreciably larger than the contact width $2a$, then the relief of axial stress σ_y which occurs in case (*a*) is not possible in either body and both can be regarded as half-spaces for the purpose of estimating the contact stresses. The reason for the stress concentration in this case may be appreciated when it is remembered that the compression of the two surfaces in the centre of the loaded region will not be very different from that with an infinitely long roller. At the ends, however, this same deformation has to be achieved by a load which extends in one direction only; beyond the end of the contact strip the surfaces are unloaded and their compression relaxes as indicated in Fig. 5.11(*c*). Just inside the end of the contact area the necessary compression is brought about by an increased pressure, which results in an increase in the width of the contact strip. The 'dog bone' shape of contact area has been observed experimentally.

https://doi.org/10.1017/CBO9781139171731.006 Published online by Cambridge University Press

Fig. 5.11. Roller end effects: (*a*) two coincident sharp ends, (*b*) one sharp end, (*c*) rounded end.

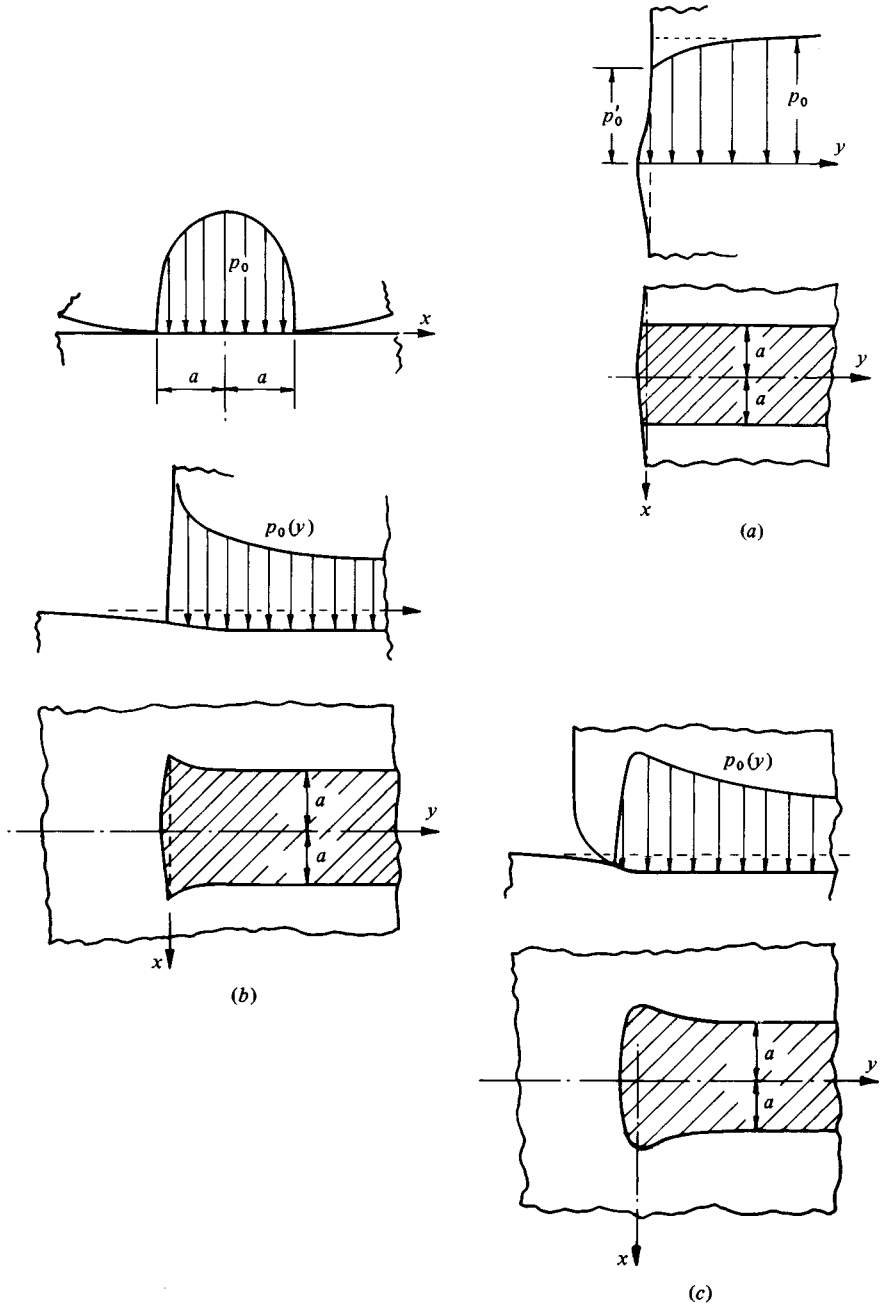

https://doi.org/10.1017/CBO9781139171731.006 Published online by Cambridge University Press

To reduce the stress concentration at the ends, the axial profile of the roller should be slightly barrelled. In theory, optimum conditions would be achieved if the contact pressure were uniform along the length. Lundberg (1939) has investigated this situation. A Hertzian distribution of pressure

$$p(x, y) = (P/\pi a l)\{1 - (x/a)^2\}^{1/2} \tag{5.60}$$

is assumed to act on a rectangular contact area of width $2a$ and length $2l$, where $l \gg a$ and a is given by the Hertz theory (eq. (4.43)). The compression at the centre of the rectangle is shown to be

$$\delta(0, 0) = \frac{P}{\pi l E^*}\{1.886 + \ln(l/a)\} \tag{5.61}$$

Along the length of the roller

$$\Delta(y) = \delta(0, 0) - \delta(0, y) \approx \frac{P}{2\pi l E^*} \ln\{1 - (y/l)^2\} \tag{5.62}$$

This expression becomes inaccurate close to the ends of the roller. At the ends themselves ($y = \pm l$)

$$\Delta(l) = \frac{P}{2\pi l E^*}\{1.193 + \ln(l/a)\} \tag{5.63}$$

Equations (5.62) and (5.63) for $\Delta(y)$ express the small correction to the axial profile of the roller required to obtain the uniform axial distribution of pressure of equation (5.60). Internal stresses due to this pressure distribution have been calculated by Kunert (1961). This profile correction, however, is difficult to manufacture and is correct only at the design load. Therefore a more general relationship between axial profile and pressure distribution is of practical interest. Over most of the length of the roller the pressure distribution in the *transverse* direction may be taken to be Hertzian, but the contact width now varies along the length. Nayak & Johnson (1979) have shown that the pressure $p(0, y)$ at any point along most of the length is related to the semi-contact-width $a(y)$ at that point by the Hertz equation (4.43). At the ends, the stress distribution is three-dimensional and must be treated as such for accurate results. Some calculations along these lines have been carried out by Ahmadi, Keer & Mura (1983).

5.7 Anisotropic and inhomogeneous materials

The elastic deformation in the contact region is obtained in the Hertz theory by assuming each solid deforms as an elastic, isotropic, homogeneous half-space. If the material of either solid is anisotropic or inhomogeneous, or if their thicknesses are not large compared with the size of the contact area their compliance under the contact pressure will differ from that assumed in the

https://doi.org/10.1017/CBO9781139171731.006 Published online by Cambridge University Press

classical theory. Practical examples of contact between anisotropic solids are found with single crystals and extruded polymer filaments; between inhomogeneous materials with foundations built on stratified rock or soil.

(a) Anisotropy

Detailed discussion of the contact of anisotropic solids is beyond the scope of this book, but an important result has been demonstrated by Willis (1966) which should be mentioned. Willis considers the contact of two non-conforming bodies of general shape under the conditions for which the Hertz theory applies except that the two solids have general anisotropy. He shows that *the contact area is still elliptical in shape and that the pressure distribution is semi-ellipsoidal* (eq. (3.58)). However, the direction of the axes of the ellipse of contact are not determined solely by the geometry of the surface profiles, but depend also upon the elastic constants. In the special case of transversely anisotropic solids (five independent elastic constants), which are in contact such that their axes of symmetry are both parallel to the common normal at the point of contact, analytical solutions for the contact stresses and deformations can be obtained with hardly more difficulty than for isotropic solids (see Turner, 1980).

Two-dimensional anisotropic contact problems are discussed by Galin (1953) and the indentation of an anisotropic half-space by a rigid punch is solved in Green & Zerna (1954). Equation (5.57) for the compression of a cylinder has been extended by Pinnock *et al.* (1966) to a transversely anisotropic polymer filament and used to determine the values of the appropriate elastic constants by measuring the diametral compression of the filament. A full discussion of anisotropy may be found in the book by Gladwell (1980, Chap. 12).

(b) Inhomogeneity

Inhomogeneous materials are of interest in soil mechanics in the calculation of the settlement of foundations. The elastic modulus of soil usually increases with depth below the surface and a particularly simple analysis is possible for an incompressible elastic half-space ($\nu = 0.5$) whose elastic moduli increase in direct proportion to the depth, i.e.

$$G = \tfrac{1}{3}E = mz \tag{5.64}$$

where m is a material constant. Calladine & Greenwood (1978) show in a simple way that the stress fields produced by a concentrated line load or a concentrated point load are the same as those found in a homogeneous half-space, given by equations (2.14) and (3.19) respectively. The displacements in the inhomogeneous material are different, however, being purely radial, given by $u_r = P/2\pi mr$ for the line load and $u_\rho = P/4\pi m\rho^2$ for the point load. It follows that

https://doi.org/10.1017/CBO9781139171731.006 Published online by Cambridge University Press

a half-space of such a material behaves like a simple Winkler elastic foundation in which the normal displacement $\bar{u}_z$ at any point on the surface is directly proportional to the pressure applied at that point, with a stiffness $2m$. Thus a long rigid foundation, of width $2a$ and weight W per unit length, resting on a half-space of this material would depress the surface by $W/4am$. The stress distribution beneath the foundation would be that found in a homogeneous half-space due to a uniform pressure $p = W/2a$ given by equations (2.27).

5.8 Layered solids, plates and shells

(a) The elastic layer

The contact of solids which have surface layers whose elastic properties differ from the substrate frequently occurs in practice; for example, the rubber covered rollers which are widely used in processing machinery. The basic situation is illustrated in Fig. 5.12(*a*) in which body (2) is in contact with the surface layer (1) on substrate (3). If the thickness b of the layer is large compared with the contact size $2a$, then the substrate has little influence and the contact stresses between (1) and (2) are given by the Hertz theory. In this section we are concerned with the situation in which b is comparable with or less than $2a$. The behaviour then depends on the nature of the attachment of the layer to the substrate. There are various possibilities: (*a*) the layer may maintain contact with the substrate at all points, but be free to slip without frictional restraint; (*b*) at the other extreme the layer may be bonded to the substrate; (*c*) slip may occur when the shear traction at interface exceeds limiting friction; and (*d*) the layer, initially in complete contact with the substrate, may partially lift from the substrate under load. The non-conforming contact between the layer and body (2) may also be influenced by frictional traction. Even if the elastic constants are the same (i.e. $E_1 = E_2, \nu_1 = \nu_2$) the limited thickness of the layer results in a relative tangential displacement at the interface which will be resisted by friction. Most analyses at the present time, however, assume the contact to be frictionless and are restricted to either the plane-strain conditions of line contact, or the axi-symmetric contact of solids of revolution in which the contact area is circular. We shall discuss the plane-strain situation first.

If the contact width is small compared with the radii of curvature of the bodies, the curvature of the layer can be ignored in analysing its deformation and the solids (2) and (3) can be taken to be elastic half-spaces.

In the case where the layer is everywhere in contact with a rigid frictionless substrate, the boundary conditions at the layer-substrate interface are $\tau_{xz} = 0$ and $u_z = 0$. The stresses in the layer are then the same as in one half of a layer of thickness $2b$ to which identical pressure distributions are applied to the opposing faces (Fig. 5.12(*b*)). The stresses in the layer are best expressed in

https://doi.org/10.1017/CBO9781139171731.006 Published online by Cambridge University Press

terms of Fourier Integral Transforms, for which the reader is referred to the books by Sneddon (1951) and Gladwell (1980, Chap. 11). In this case, with an *even* distribution of pressure applied symmetrically to each surface $z = \pm b$, Sneddon shows that the normal displacement of each surface is given by

$$\bar{u}_z = \frac{4(1-\nu_1^2)}{\pi E_1} \int_0^\infty \left(\frac{2 \sinh^2 \alpha b}{2\alpha b + \sinh 2\alpha b} \right) \tilde{p}(\alpha) \frac{\cos \alpha x}{\alpha} \, d\alpha \qquad (5.65)$$

Fig. 5.12

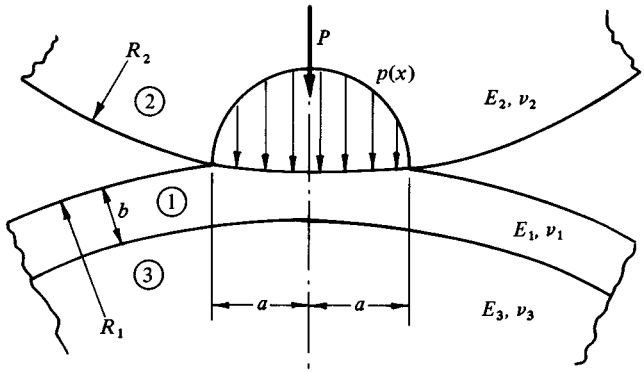

(*a*)

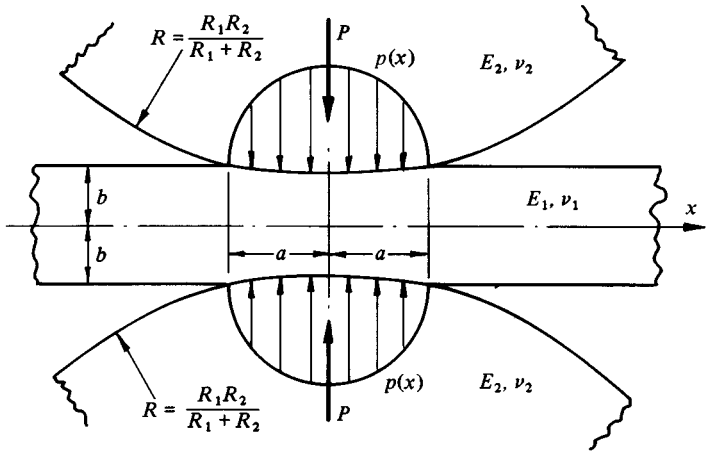

(*b*)

https://doi.org/10.1017/CBO9781139171731.006 Published online by Cambridge University Press

where $\bar{p}(\alpha)$ is the Fourier Cosine Transform of the pressure $p(x)$, i.e.

$$\bar{p}(\alpha) = \int_0^\infty p(x) \cos \alpha x \, dx \tag{5.66}$$

Comparable expressions to (5.65) in terms of $\bar{p}(\alpha)$ are given by Sneddon for the tangential displacement $\bar{u}_x$ and for the components of stress σ_x, σ_z and τ_{zx} throughout the layer. If the layer is bonded to the substrate the expression for $\bar{u}_z$ corresponding to (5.65) is given by Bentall & Johnson (1968).

For a uniform pressure p distributed over an interval $-c < x < c$, equation (5.66) gives:

$$\bar{p}(\alpha) = (p/\alpha) \sin(\alpha c) \tag{5.67}$$

For a triangular distribution of pressure of peak value p_0,

$$\bar{p}(\alpha) = \frac{2p_0}{c\alpha^2} \sin^2\left(\frac{c\alpha}{2}\right) \tag{5.68}$$

In the limit, as $c \to 0$, the transform of a concentrated force P is $P/2$. Frictional tractions $q(x)$ on the faces of the layer can be handled in the same way (see Bentall & Johnson, 1968).

The awkward form of the integrand in equation (5.65) and associated expressions has led to serious difficulties in the analysis of contact stresses in strips and layers. Two approaches have been followed. In one the integrand is approximated by an asymptotic form which is appropriate for either thin strips ($b \ll a$), or thick strips ($b \gg a$) (Meijers, 1968; Alblas & Kuipers, 1970). In the other approach the pressure distribution $p(x)$ is built up of discrete elements each of a width $2c$. These may be elements of uniform pressure whose transform is given by equation (5.67) (Conway *et al.*, 1966, 1969) or may be overlapping triangular elements as given by equation (5.68) (Bentall & Johnson, 1968). The use of overlapping triangular elements gives rise to a piecewise linear distribution of pressure; the application of this technique to the contact of solid bodies is described in the next section.

The indentation by a rigid frictionless cylinder of an elastic layer which is supported on a rigid plane surface has been studied by various workers (*a*) for a layer which is bonded to the rigid base and (*b*) for a layer which can slip on the base without friction. The difference between these two cases is significant when the material of the layer is incompressible ($\nu = 0.5$). Solutions for relatively thick layers ($b > a$) have been given by Pao *et al.* (1971) and by Meijers (1968), and for thin layers ($b < a$) by Alblas & Kuipers (1970) and Meijers (1968).

In the limit when $b \ll a$, the state of affairs can be analysed in an elementary way. A thin layer indented by a frictionless rigid cylinder is shown in Fig. 5.13. If $b \ll a$ it is reasonable in the first instance to assume that the deformation

https://doi.org/10.1017/CBO9781139171731.006 Published online by Cambridge University Press

through the layer is homogeneous, i.e. plane sections remain plane after compression as shown in Fig. 5.13(*a*), so that the stress σ_x is uniform through the thickness. We will consider first the case of no friction at the interface between the layer and the rigid substrate, whereupon $\sigma_x = 0$ throughout.

In plane strain

$$\epsilon_z = \frac{1-\nu^2}{E}\,\sigma_z = -\frac{1-\nu^2}{E}\,p(x) \tag{5.69}$$

The compressive strain in the element is given by the geometry of deformation:

$$\epsilon_z = -(\delta - x^2/2R)/b \tag{5.70}$$

Since the pressure must fall to zero at $x = \pm a$, equations (5.69) and (5.70) give $\delta = a^2/2R$ and

$$p(x) = \frac{E}{1-\nu^2}\,\frac{a^2}{2Rb}\,(1-x^2/a^2) \tag{5.71}$$

whence the load

$$P = \tfrac{2}{3}\,\frac{E}{1-\nu^2}\,\frac{a^3}{Rb} \tag{5.72}$$

In the case where the layer is bonded to the substrate and plane sections remain plane, the strain ϵ_x is zero throughout, i.e.

$$\epsilon_x = \frac{1-\nu^2}{E}\left\{\sigma_x + \frac{\nu}{1-\nu}\,p(x)\right\} = 0$$

Fig. 5.13. An elastic layer on a rigid substrate indented by a rigid cylinder: (*a*) Poisson's ratio $\nu < 0.45$; (*b*) $\nu = 0.5$.

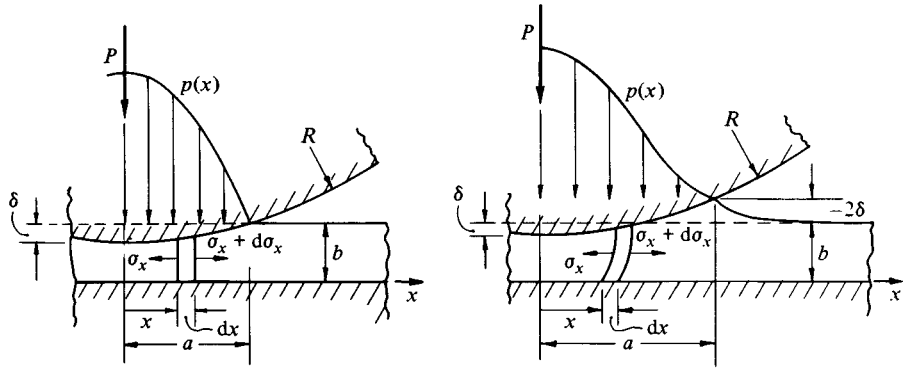

https://doi.org/10.1017/CBO9781139171731.006 Published online by Cambridge University Press

In this case

$$\epsilon_z = \frac{1-\nu^2}{E}\left\{-p(x) - \frac{\nu}{1-\nu}\sigma_x\right\}$$

Eliminating σ_x and substituting for ϵ_z from (5.70) gives

$$p(x) = \frac{(1-\nu)^2}{1-2\nu}\,\frac{E}{1-\nu^2}\,\frac{a^2}{2Rb}\,(1-x^2/a^2) \tag{5.73}$$

and

$$P = \tfrac{1}{3}\,\frac{(1-\nu)^2}{1-2\nu}\,\frac{E}{1-\nu^2}\,\frac{a^3}{Rb} \tag{5.74}$$

For an incompressible material ($\nu = 0.5$) equation (5.73) implies an infinite contact pressure, showing that the assumption that plane sections remain plane is inappropriate in this case. However, by permitting the cross-sections of the layer to deform into a parabola (i.e. u_x to be second order in z as shown in Fig. 5.13(b)), it may be shown that for a thin layer of an incompressible material:

$$p(x) = \frac{Ea^4}{24Rb^3}\,(1-x^2/a^2)^2 \tag{5.75}$$

$$P = \frac{2Ea^5}{45Rb^3} \tag{5.76}$$

$$\delta = a^2/6R \tag{5.77}$$

The relationship between contact width and load for different ratios of layer thickness b to semi-contact width a is illustrated in Fig. 5.14, by plotting a/a_∞ against b/a, where $a_\infty{}^2 = 4PR(1-\nu^2)/\pi E$ = the Hertz semi-contact width ($b/a \to \infty$). The full curves are from Meijers (1968) and show the difference between $\nu = 0.3$ and $\nu = 0.5$. The asymptotic expressions for $b \ll a$, given by equations (5.74) and (5.76) are plotted for comparison.

The pressure distribution given by (5.75) is different from that for a compressible material (5.73). It has a zero gradient at the edges of the contact as shown in Fig. 5.13(b). The change in behaviour takes place quite rapidly in the range of Poisson's ratio between 0.45 and 0.48. The contact pressure varies as $(b/a)^{-3}$ so that it becomes high when the layer is very thin; the deformation of the indenter or the substrate can then no longer be neglected. Stresses in an elastic layer on an *elastic* substrate have been analysed by Gupta *et al.* (1973, 1974) and Barovich *et al.* (1964); see also §10.1.

Axi-symmetrical stresses in a layer or sheet have been expressed in terms of Hankel transforms by Sneddon (1951). The general features are similar to those

https://doi.org/10.1017/CBO9781139171731.006 Published online by Cambridge University Press

found in plane deformation; a formal relationship between the two is discussed by Gladwell (1980), Chap. 10. Asymptotic solutions for the stresses in a layer due to a frictionless indenter have been found by Aleksandrov (1968, 1969) for thick and thin layers respectively. The contact of a flat circular punch and sphere with an elastic layer including the effects of friction has been analysed by Conway & Engel (1969) using the numerical method. For layers bonded to a substrate Matthewson (1981) has obtained an asymptotic solution for thin layers including the shear stress in the bond; McCormick (1978) has considered circular and elliptical contact areas for plates of general thickness.

(b) Receding contacts

This book is almost entirely concerned with the contact of non-conforming solids which touch initially at a point or along a line and whose area of contact grows with increasing load. Closely conforming contacts, on the other hand, which touch initially over an appreciable area when loaded may deform such that the contact area decreases. For example a perfectly fitting pin in a hole will initially touch round the whole of its circumference but, when it is loaded perpendicular to its axis, a gap will appear between the pin and the hole on the unloaded side. If the loaded contact area is completely contained within the unloaded contact area, the situation is described as *receding contact*,

Fig. 5.14. Contact width of an elastic layer on a rigid substrate indented by a rigid cylinder. Solid line – Meijers (1968); broken line – asymptotic solutions for $b \ll a$, eq. (5.74) and eq. (5.76); chain line – Hertz ($b \gg a$).

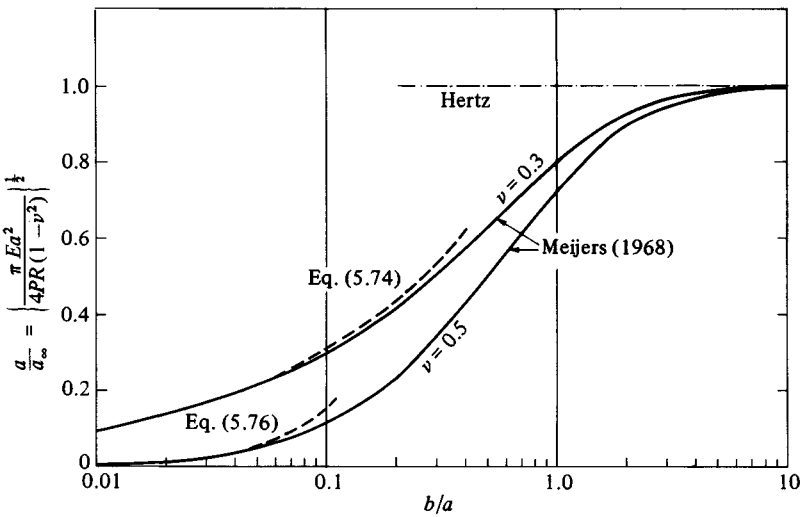

https://doi.org/10.1017/CBO9781139171731.006 Published online by Cambridge University Press

and has been shown by Tsai *et al.* (1974) and Dundurs (1975) to have special properties:

(i) The contact area changes discontinuously from its initial to its loaded shape and size on application of the first increment of load,
(ii) if the load increases in magnitude, but does not change in disposition, the contact area does not change in shape or size, and
(iii) the displacements, strain and stresses increase in direct proportion to the load.

The layer and the substrate shown in Fig. 5.15 will give rise to a receding contact if the layer is free to lift off the substrate under the action of the concentrated load P. Gladwell (1976) investigated this problem treating the layer as a simple beam in bending. Neglecting its own weight the beam was shown to make contact with the substrate under load over a distance $2c$, independent of the load, given by

$$(c/b)^3 = 1.845 \left\{ \frac{1-\nu_3^2}{E_3} \Big/ \frac{1-\nu_1^2}{E_1} \right\} = 1.845 \frac{1-\alpha}{1+\alpha} \tag{5.78}$$

where α is defined by equation (5.3*a*). Keer *et al.* (1972) solved the same problem using the proper elastic equations for a layer. The width of the contact between the layer and the substrate was found to be close to that given by equation (5.78) except when α was close to ± 1.0, i.e. when either the substrate or the layer was comparatively rigid. Ratwani & Erdogan (1973) have examined the situation where a layer which is free to lift is indented by a rigid cylinder ($E_2 \to \infty$) as shown in Fig. 5.12(*a*). At light loads, when $a \ll b$, the situation is much the same as for loading by a concentrated force and the semi-contact width c between the layer and substrate is given approximately by equation (5.78). When a grows with load to be comparable with b, c is no longer constant. Keer *et al.* (1972) have also examined axi-symmetric receding contact between a layer and an elastic half-space.

Fig. 5.15

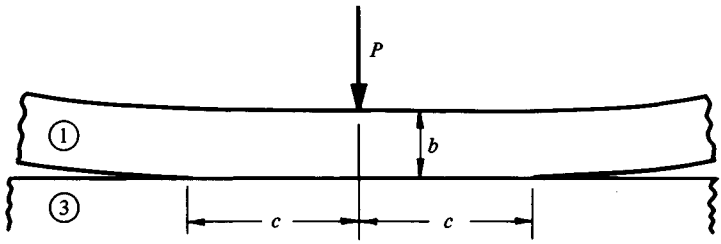

https://doi.org/10.1017/CBO9781139171731.006 Published online by Cambridge University Press

(c) Plates and shells

Thin plates or shell-like bodies in contact react to the contact load by bending. Thus bending stresses are added to the contact stresses. A discussion of the stresses in the vicinity of a concentrated load acting on a beam is given by Timoshenko & Goodier (1951, p. 99). When the beam or plate is relatively thick we can regard the stress field as comprising the superposition of Hertzian contact stresses and simple bending stresses. The bending action introduces a compressive stress in the upper layers of the plate which will add to the longitudinal component of the contact stress field (eq. (4.46*a*)) which is also compressive. The effect is to reduce the maximum value of the principal shear stress (eq. (4.47)) and to delay the initiation of plastic yield. When the plate is thin compared with the size of the contact area, the stresses are predominantly due to bending. For example, consider a rigid cylinder of radius R which is pressed into contact with a flat plate of length $2l$, width w and thickness $2b$, such that the contact arc is $2a$, where $b \ll a \ll R$ (see Fig. 5.16). The contact loading can be found by the elementary theory of bending. Within the contact arc the plate is bent into a circular arc of radius R, through the action of a uniform bending moment:

$$M = 2Ewb^3/3R(1-\nu^2)$$

For the bending moment to be constant within the arc of contact, the contact pressure must comprise two concentrated forces at its edges and be zero elsewhere, whereupon

$$\tfrac{1}{2}P(l-a) = 2Ewb^3/3R(1-\nu^2) \tag{5.79}$$

This equation determines the length of the arc of contact due to a given load P. This simple example shows that, as the load is progressively increased from first contact, so that the arc of contact grows from being small to large compared with the thickness of the plate, the contact pressure distribution changes from having

Fig. 5.16

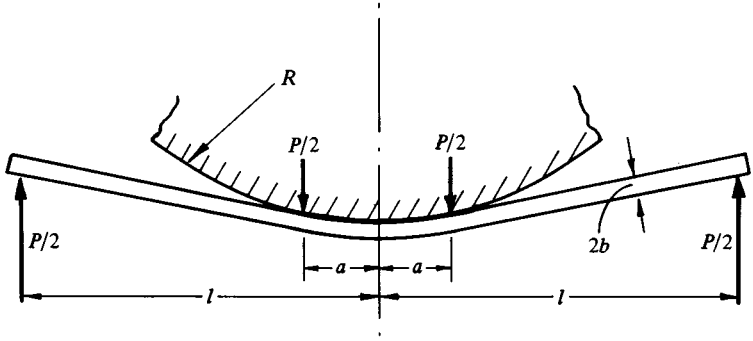

https://doi.org/10.1017/CBO9781139171731.006 Published online by Cambridge University Press

a maximum in the centre to one in which the pressure is concentrated at the edges. When the deformations are large it is necessary to take the changes in geometry into account and to make use of the theory of the 'Elastica' (see Wu & Plunkett, 1965).

Axi-symmetric contact of a paraboloid with a thin plate has been studied by Essenburg (1962) and the compression of a thin spheroidal shell between two rigid flats by Updike & Kalnins (1970, 1972). The use of classical plate and shell theory, in which shear deformation is ignored, leads to the contact pressure being concentrated into a ring of force at the edge of the circle of contact similar to the bent plate shown in Fig. 5.16. To obtain a more realistic distribution of contact pressure it is necessary to include the shear stiffness of the plate or shell. For thin plates, however, the pressure is still a minimum in the centre, rising to a maximum at the edges (see Gladwell & England, 1975).

A spheroidal shell, unlike a cylindrical shell, is not a developable surface. When pressed into contact with a frictionless flat surface, the shell is initially flattened, which introduces a compressive membrane stress. When a critical compression is reached, the shell buckles in the contact zone by the formation of a dimple. Updike & Kalnins (1970, 1972) investigate the onset of instability and discuss the conditions under which buckling will precede plastic yielding and vice versa.

5.9 Numerical methods

Many non-Hertzian contact problems do not permit analytical solutions in closed form. This is particularly true in the case of conforming contacts where the initial separation cannot be described by a simple quadratic expression (eq. (4.3)) and also in problems with friction involving partial slip. It has led to the development of various numerical methods which we shall discuss in this section. The essence of the problem is to determine the distributions of normal and tangential tractions which satisfy the normal and tangential boundary conditions at the interface, both inside and outside the contact area whose shape and size may not be known at the outset. In general the normal and tangential tractions are coupled, but we saw in §4 that considerable simplification can be achieved, with only a small loss of precision, by neglecting the effect upon the normal pressure of the tangential traction which arises when the materials of the two bodies are different. Thus the normal pressure is found on the assumption that the surfaces are *frictionless.* The internal stresses, if required, are found after the surface tractions are known.

The classical method, which has been applied to line contact and axi-symmetric problems in which the shape of the contact area is known, is to represent the pressure distribution by an infinite series of known functions. The series

is then truncated to satisfy the boundary conditions approximately. Although a continuous distribution of traction is obtained, this method is basically ill-conditioned and can lead to large errors unless the functions are chosen carefully. The series due to Steuermann described in §3 provide examples of this method.

Modern computing facilities generally favour a different approach in which continuous distributions of traction are replaced by a discrete set of 'traction elements' and the boundary conditions are then satisfied at a discrete number of points - the 'matching points'. The simplest representation of a traction distribution is an array of concentrated normal or tangential forces as shown in Fig. 5.17(*a*). The difficulty with this representation lies in the infinite surface

Fig. 5.17. Discrete pressure elements (*a*) concentrated forces, (*b*) uniform (piecewise constant), (*c*) overlapping triangles (piecewise linear).

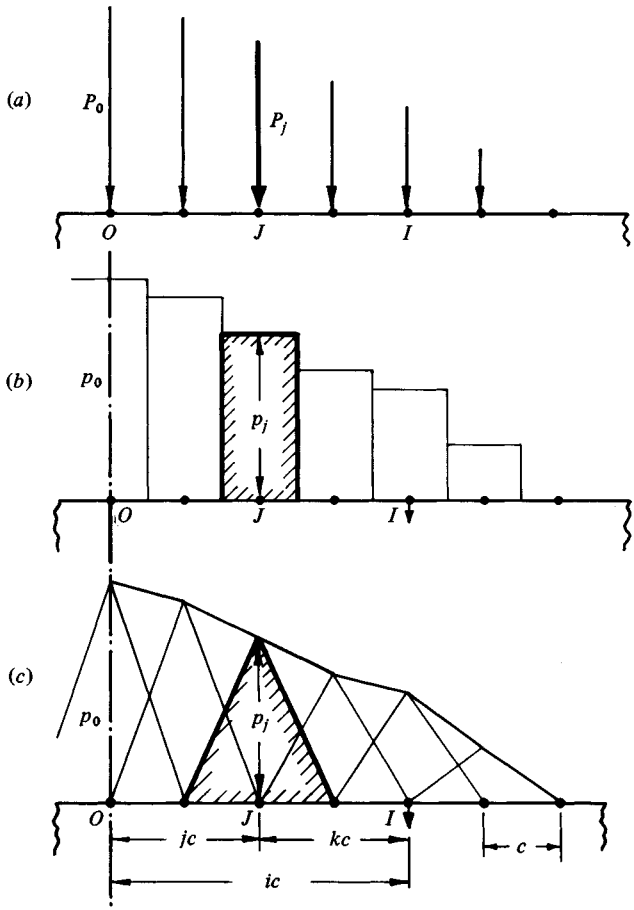

https://doi.org/10.1017/CBO9781139171731.006 Published online by Cambridge University Press

displacement which occurs at the point of application of a concentrated force. This difficulty is avoided if the traction is represented by adjacent columns of *uniform* traction acting on discrete segments of the surface, which give rise to a *stepwise* distribution as shown in Fig. 5.17(*b*). The surface displacements are now finite everywhere, but the displacement gradients are infinite between adjacent elements, where there is a step change in traction. A *piecewise-linear* distribution of traction, on the other hand, produces surface displacements which are everywhere smooth and continuous. Such a distribution of traction in line (two-dimensional) contact may be built up by the superposition of overlapping triangular traction elements, as shown in Fig. 5.17(*c*). The corresponding traction element in three-dimensional contact is a regular pyramid on an hexagonal base, as shown in Fig. 5.18. An array of such pyramids, erected on an equilateral triangular mesh and overlapping, so that every apex coincides with a mesh point,

Fig. 5.18. Overlapping hexagonal pressure elements on an equilateral triangular (ξ, η) base.

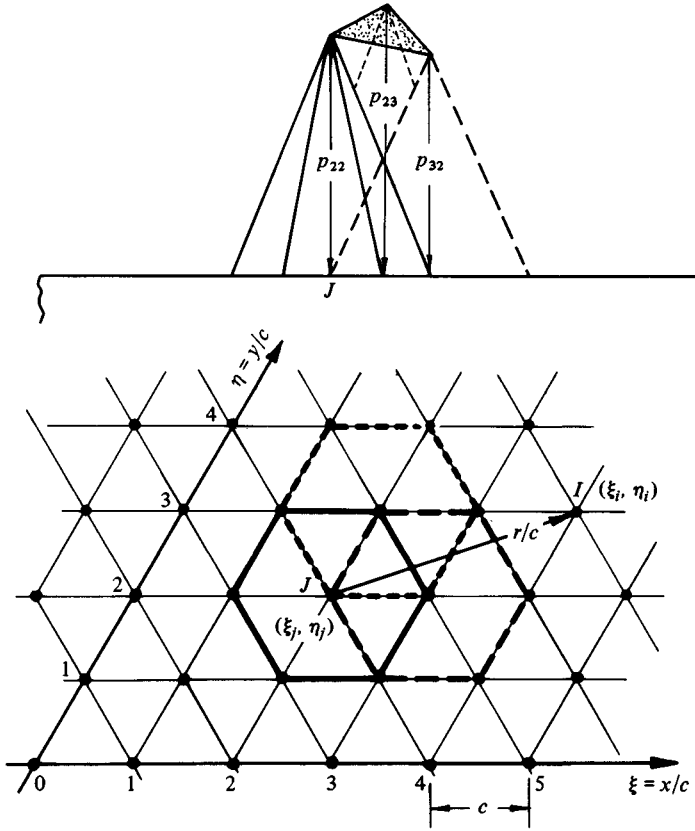

https://doi.org/10.1017/CBO9781139171731.006 Published online by Cambridge University Press

adds up to a resultant distribution of traction comprising plane triangular facets. One such facet based on the points (2, 2), (3, 2) and (2, 3) is shown in Fig. 5.18. The traction distributions are then specified completely by the discrete values p_j of the traction elements.

In order to find the values of the traction elements which best satisfy the boundary conditions two different methods have been developed:

(*a*) the direct, or Matrix Inversion, method in which the boundary conditions are satisfied exactly at specified 'matching points', usually the mid-points of the boundary elements, and

(*b*) the Variational method in which the values of the traction elements are chosen to minimise an appropriate energy function.

In describing the two methods we shall consider the normal contact of frictionless solids whose profiles are arbitrary and of such a form that they cannot be adequately characterised by their radii of curvature at their point of first contact. The gap between the two surfaces before deformation, however, is known and is denoted by the function $h(x, y)$ which, in the first instance, we shall assume to be smooth and continuous. It then follows from the principle discussed in §1 that the contact pressure falls continuously to zero at the edge of the contact. The elastic displacements of corresponding points on the two surfaces then satisfy the relationship:

$$\bar{u}_{z1} + \bar{u}_{z2} + h(x, y) - \delta \begin{cases} = 0 \text{ within contact} & (5.80a) \\ > 0 \text{ outside contact} & (5.80b) \end{cases}$$

where δ is the approach of distant reference points in the two bodies.

Whichever method is used, it is first necessary to choose the form of pressure element and to divide the contact surface into segments of appropriate size. Referring to Fig. 5.17, the matrix of influence coefficients C_{ij} is required, which expresses the displacement at a general point I due to a unit pressure element centred at point J. The total displacement at I is then expressed by

$$\{\bar{u}_z\}_i = -\frac{(1-\nu^2)c}{E} \sum C_{ij} p_j \qquad (5.81)$$

Difficulty arises in line contact (plane strain) where the displacements are undefined to the extent of an arbitrary constant. The difficulty may be overcome by taking displacements relative to a datum point, which is conveniently chosen to be the point of first contact, i.e. the origin. Since $h(0) = 0$, equation (5.80*a*) may be rewritten for line contact as

$$\{\bar{u}_{z1}(0) - u_{z1}(x)\} + \{\bar{u}_{z2}(0) - \bar{u}_{z2}(x)\}$$

$$-h(x) \begin{cases} = 0 \text{ within contact} & (5.82a) \\ > 0 \text{ outside contact} & (5.82b) \end{cases}$$

https://doi.org/10.1017/CBO9781139171731.006 Published online by Cambridge University Press

and we rewrite equation (5.81):

$$\{\bar{u}_z(0) - \bar{u}_z(x)\}_i = \frac{1-\nu^2}{E}\, c \sum B_{ij} p_j \tag{5.83}$$

where $B_{ij} \equiv C_{0j} - C_{ij}$.

For a uniform pressure element in plane strain, the influence coefficients are obtained from equation (2.30*d*) by replacing a by c and x by kc, with the result:

$$C_{ij}(k) = \frac{1}{\pi}\{(k+1)\ln(k+1)^2 - (k-1)\ln(k-1)^2\} + \text{const.} \tag{5.84}$$

where $k = i - j$. For a triangular pressure element the influence coefficients are obtained from equations (2.37*c*), whereby

$$C_{ij}(k) = \frac{1}{2\pi}\{(k+1)^2 \ln(k+1)^2 + (k-1)^2 \ln(k-1)^2 - 2k^2 \ln k^2\} + \text{const.} \tag{5.85}$$

For point contacts, the influence coefficients for uniform pressure elements acting on rectangular segments of the surface ($2a \times 2b$) can be obtained from equations (3.25) by replacing x by $(x_i - x_j)$ and y by $(y_i - y_j)$. Pyramidal pressure elements are based on a grid with axes $x(=\xi c)$ and $y(=\eta c)$ inclined at 60° as shown in Fig. 5.18. The distance JI is given by

$$JI \equiv r = ck = c\{(\xi_i - \xi_j)^2 + (\xi_i + \xi_j)(\eta_i - \eta_j) + (\eta_i - \eta_j)^2\}^{1/2} \tag{5.86}$$

The influence coefficients are found by the method described in §3.3. At the centre of the pyramid ($i = j$): $C_{ij}(0) = (3\sqrt{3}/2\pi)\ln 3 = 0.9085$; at a corner $C_{ij}(1) = \frac{1}{3}C_{ij}(0)$. For values of $k^2 > 1$ the coefficient can be found by replacing the pyramid by a circular cone of the same volume, i.e. which exerts the same load, with the results shown in Table 5.2. For values of $k^2 > 9$ it is sufficiently accurate (<0.5% error) to regard the pyramid as a concentrated force, so that $C_{ij}(k) = \sqrt{3}/2\pi$.

Table 5.2

$\xi_i - \xi_j, \eta_i - \eta_j$	1,1	2,0	2,1	3,0
k^2	3	4	7	9
$C_{ij}(k)$	0.1627	0.1401	0.1051	0.0925

https://doi.org/10.1017/CBO9781139171731.006 Published online by Cambridge University Press

The total load P carried by the contact is related to the values of the pressure elements by

$$P = A \sum p_j \tag{5.87}$$

where A is a constant depending upon the form and size of the pressure element. For a uniform pressure element A is the surface area of the element; for a pyramidal element, $A = \sqrt{3}c^2/2$. We are now in a position to discuss the methods for finding the values of p_j.

(a) Matrix inversion method

The displacements $\{\bar{u}_z\}_i$ at a general mesh point I are expressed in terms of the unknown pressures p_j by equation (5.81) for point contact and equation (5.83) for line contact. If n is the number of pressure elements, i and j take integral values from 0 to $(n-1)$. Substituting these displacements into equations (5.80*a*) and (5.82*a*) respectively gives

$$\sum_{j=0}^{j=n-1} C_{ij} p_j = (E^*/c)(h_i - \delta) \tag{5.88}$$

for point contacts and

$$\sum_{j=0}^{j=n-1} B_{ij} p_j = (E^*/c) h_i \tag{5.89}$$

for line contacts. If the compression δ is specified then equation (5.88) can be solved directly by matrix inversion for the n unknown values of p_j. It is more likely, however, that the total load P is specified. The compression δ then constitutes an additional unknown, but an additional equation is provided by (5.87). In equation (5.88) for line contacts the origin ($i = 0$) is a singular point since $B_{0j} = h_0 = 0$, but again equation (5.87) for the total load provides the missing equation.

It is unlikely in problems requiring numerical analysis that the shape or size of the contact area is known in advance. To start, therefore, a guess must be made of the shape of the contact surface and its size must be chosen to be sufficiently large to enclose the true area. Where the value of δ is specified or can be estimated, a first approximation to the contact area can be obtained from the 'interpenetration curve', that is the contour of separation $h(x, y) = \delta$. This is the area which is divided into an array of n pressure elements. After solving equation (5.88) or (5.89) for the unknown pressures, it will be found that the values of p_j near to the periphery are negative, which implies that a tensile traction is required at some mesh points to maintain contact over the whole of the assumed area. For the second iteration these mesh points are excluded from the assumed contact area and the pressures there put equal to zero. Experience

https://doi.org/10.1017/CBO9781139171731.006 Published online by Cambridge University Press

confirms that repeated iterations converge to a set of values of p_j which are positive or zero and which satisfy equation (5.80*a*) within the region where $p_j > 0$ and equation (5.80*b*) in the region where $p_j = 0$. The boundary between the two regions defines the contact area to the accuracy of the mesh size.

In line contact the contact area is the strip $-b \leqslant x \leqslant a$ where, for a given load, a and b remain to be found. If the deformation is symmetrical about the origin, so that $b = a$, the pressure distribution can be found without iteration. It is preferable to take a as the independent load variable, to divide the contact strip into $2n$ segments and to use $2n - 1$ overlapping triangular pressure elements as shown in Fig. 5.17(*c*). This arrangement automatically ensures that the contact pressure falls to zero at $x = \pm a$. Equation (5.83) can then be inverted directly to find the values of p_j. This method has been used by Paul & Hashemi (1981) for normal contact and by Bentall & Johnson (1967) for problems in which tangential as well as normal tractions are present.

The procedure outlined above is appropriate for bodies whose profiles are both smooth and continuous. If one of the bodies has a sharp corner at the edge of the contact, the pressure at the edge of contact, instead of falling to zero, will rise to infinity according to $\rho^{-\lambda}$, where ρ is the distance from the edge and the value of λ depends upon the elasticities of the two bodies but is approximately 0.5 (see §1). This type of contact can be incorporated into the above method by using a boundary element in the segment adjacent to the edge of contact in which the pressure varies as $\rho^{-0.5}$ as shown in Fig. 5.19. The displacement at a distance x from the edge due to such an element of pressure is

Fig. 5.19. Singular pressure element.

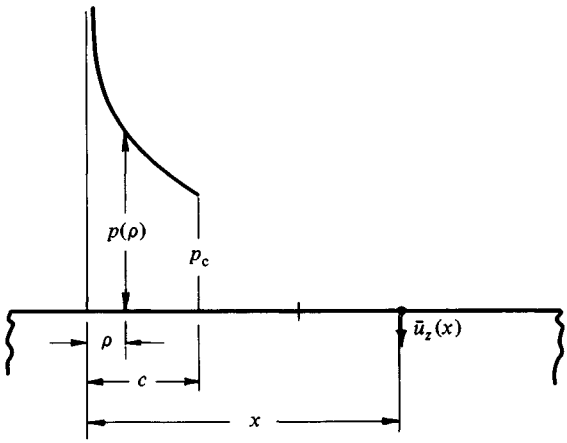

https://doi.org/10.1017/CBO9781139171731.006 Published online by Cambridge University Press

given by

$$\bar{u}_z(x) = -\frac{1-\nu^2}{\pi E}\, 2cp_c \left\{ \ln\left(\frac{x-c}{c}\right)^2 + (x/c)^{1/2} \ln\left(\frac{x^{1/2}+c^{1/2}}{x^{1/2}-c^{1/2}}\right)^2 - 4 \right\} + c \tag{5.90}$$

(b) Variational methods

Variational methods have been applied to non-Hertzian contact problems for two reasons: (i) to establish conditions which will determine the shape and size of the contact area and the contact stresses uniquely and (ii) to enable well-developed techniques of optimisation such as quadratic programming to be used in numerical solutions.

Fichera (1964) and Duvaut & Lions (1972) have investigated general principles which govern the existence and uniqueness of solution to contact problems. For two bodies having continuous profiles, pressed into contact by an overall displacement δ, Duvaut & Lions show that the true contact area and surface displacements are those which minimise the total strain energy U_E (with δ kept constant), provided that there is no interpenetration, i.e. provided

$$\bar{u}_{z1} + \bar{u}_{z2} + h(x,y) - \delta \geqslant 0$$

everywhere. An example of the application of this principle to a Hertz contact was given in §5.

For numerical solution of contact problems it is more convenient to work in terms of unknown tractions rather than displacements. Kalker (1977, 1978) has therefore proposed an alternative principle in which the true contact area and distribution of surface traction are those which minimise the total complementary energy (V^*), subject to the constraint that the contact pressure p is everywhere positive. Now the total complementary energy can be written:†

$$V^* = U_E^* + \int_S p(h-\delta)\, dS \tag{5.91}$$

where S is the surface on which p acts and U_E^* is the internal complementary energy of the two stressed bodies. For linear elastic materials the complementary energy U_E^* is numerically equal to the elastic strain energy U_E, which can be expressed in terms of the surface tractions and displacements by

$$U_E^* = U_E = \tfrac{1}{2}\int_S p(\bar{u}_{z1} + \bar{u}_{z2})\, dS \tag{5.92}$$

† For a discussion of the complementary energy principle see T. H. Richards, *Energy methods in stress analysis*, Ellis Horwood, 1977, p. 256.

https://doi.org/10.1017/CBO9781139171731.006 Published online by Cambridge University Press

To obtain a numerical solution the prospective contact area S is subdivided into a mesh on which elements of pressure act. Using equation (5.81) we have

$$U_{\mathrm{E}}^{*} = -\frac{(1-\nu^2)cA}{2E^{*}} \sum\{\sum C_{ij}p_j\}p_i \tag{5.93}$$

and

$$\int_S p(h-\delta)\,\mathrm{d}S = A \sum p_i(h_i-\delta) \tag{5.94}$$

where A is defined in equation (5.87). Thus substituting from (5.93) and (5.94) into (5.91) gives V^* as an object function quadratic in p_i. The values of p_i which minimise V^*, subject to $p_i > 0$, can be found by using a standard quadratic programming routine, e.g. that of Wolfe (1959) or Beale (1959). The contact is then defined, within the precision of the mesh size, by the boundary between the zero and non-zero pressures. This method has been applied to frictionless non-Hertzian contact problems by Kalker & van Randen (1972).

To find the subsurface stresses it is usually adequate to represent the surface tractions by an array of concentrated forces as in Fig. 5.17(*a*). The stress components at any subsurface point can then be found by superposition of the appropriate expressions for the stresses due to a concentrated force, normal or tangential, given in §§2.2 & 3 or §§3.2 & 6.

When the size of the contact region is comparable with the leading dimensions of one or both bodies, influence coefficients based on an elastic half-space are no longer appropriate. Bentall & Johnson (1968) have derived influence coefficients for thin layers and strips but, in general, a different approach is necessary. The finite-element method has been applied to contact problems, including frictional effects, notably by Fredriksson (1976). A more promising technique is the Boundary Element Method which has been applied to two-dimensional contact problems by Andersson *et al.* (1980).